 © 2015 Russian Academy of Sciences and Turpion Ltd

DOI 10.1070/RCR4452

Cadmium sulfide nanoparticles prepared by chemical bath deposition

N S Kozhevnikova,[a] A S Vorokh,[a] A A Uritskaya [a, b]

[a] Institute of Solid State Chemistry, Ural Branch of the Russian Academy of Sciences
ul. Pervomaiskaya 91, 620990 Ekaterinburg, Russian Federation
[b] Chemical Technological Institute,
Ural Federal University named after the First President of Russia B N Yeltsin
ul. Mira 19, 620002 Ekaterinburg, Russian Federation

Key results of recent studies on cadmium sulfide nanoparticles are systematized. The dependence of the structure and properties of CdS nanoparticles on the nanoparticle size is illustrated. The possibility of utilizing CdS quantum dots as biological labels and sensitizers for solar cells is analyzed. The principles, features and potential of the method of aqueous solution deposition are described from the standpoint of synthesis of CdS nanocrystals and hybrid forms based on them with specified structure and properties.
The bibliography includes 180 references.

Contents

I. Introduction 225
II. The structure of CdS nanoparticles: between the crystalline and amorphous states 227
III. Properties of CdS nanoparticles: the size and surface effects 231
IV. Aqueous solution deposition of nanostructured forms of CdS: from thin films to colloidal systems 236
V. Conclusion 246

I. Introduction

Cadmium sulfide is traditionally used as yellow pigment called 'aurora yellow'. The search for cadmium for industrial applications revealed that it only occurs as sulfide in the greenockite mineral, a companion to sphalerite (ZnS). The discovery of semiconductor properties in CdS in the second half of the 20th century attracted the attention of researchers to this compound and was followed by the development of novel methods of synthesis using vacuum technology. This made it possible to prepare CdS films of thickness to 0.5 μm.

The next surge of interest in CdS originated from elaboration of a thin-film preparation technology based on the aqueous solution deposition. Professor G A Kitaev, a founder of the Ural scientific school of thin-film synthesis, wrote: 'It is usually accepted that the chemical method of preparation of metal chalcogenide films is more art than science... The experience accumulated by the staff of the Department of Physical and Colloid Chemistry, Ural Polytechnic Institute named after Kirov, entitles us to speak of the need to reclassify chemical methods from art to science because chemical methods can be scientifically based. This enables formulation of clear recommendations concerned with the synthesis'.[1]

Pioneering studies were carried out by chemists from the Ural Region in the 1960s. The results obtained underlie both fundamental understanding of deposition processes and development of thin-film deposition technologies which found wide industrial applications in the USSR.[2–5] Aqueous solution deposition still belongs to the most widely employed methods for synthesis of metal chalcogenides including CdS. Therefore, it is of importance to generalize and systematize information on the structure and properties of CdS nanoparticles and on the mechanisms of formation of nanostructured forms of CdS produced by this method.

N S Kozhevnikova Candidate of Chemical Sciences, Senior Researcher of the Laboratory of Inorganic Synthesis, ISSC UB RAS.
Telephone: +7(343)362 – 3564, e-mail: kozhevnikova@ihim.uran.ru
Current research interests: synthesis, structure and reactivity of metal chalcogenides, structure and properties of solutions, colloidal systems, nanoparticles.
A S Vorokh Candidate of Physical and Mathematical Sciences, Senior Researcher of the Laboratory of Quantum Chemistry and Spectroscopy at the same Institute.
Telephone: +7(343)362 – 3356, e-mail: vorokh@ihim.uran.ru
Current research interests: metal chalcogenides, structure of nanomaterials, X-ray diffraction analysis, X-ray photoelectron diffraction.
A A Uritskaya Candidate of Chemical Sciences, Senior Researcher of the Laboratory of Inorganic Synthesis at the same Institute and Associate Professor of the Chair of Physical and Colloid Chemistry at the CTI UrFU. Telephone: +7(343)375 – 4445, e-mail: uritskaya1940@mail.ru
Current research interests: chemical thermodynamics, synthesis, structure and reactivity of metal chalcogenides; colloidal systems, equilibrium and kinetics of processes in reacting chemical systems.

Received 3 March 2014
Uspekhi Khimii **84** (3) 225 – 250 (2015); translated by A M Raevskiy

To evaluate the interest of researchers in this field, we performed a bibliometric analysis of publications on CdS reported between 1980 and 2013 using the Web of Science scientific databases encompassed by the Thomson Reuters Web of Knowledge suite.

Studies with 'CdS' or 'Cadmium Sulfide' in the titles were analyzed. The distribution of publications over particular subfields was assessed by retrieving information using keywords (and their combinations) from abstracts, *e.g.*, 'nano', 'bio', 'TiO_2' and 'solar cells' ignoring other keywords. The results obtained are presented in Fig. 1.

In the last two decades, there has been renewal of interest in the chemical bath deposition of CdS (see Fig. 1, curve *5*). Since the mid-1990s to nearly 2007, curve *5* behaves very similarly to curve *4*. Interest in this method is due to the advances achieved in the deposition of nanostructured barrier layers based on CdS films for thin-film CIGSSe (Cu–In–Ga–S–Se) heterojunction solar cells with cascading effect.[6–10] Utilization of CdS thin films from 10 to 100 nm thick as the first 'window' or buffer layer in the solar cells allowed one to increase their efficiency to 19.9%.[10]

Since 2006, solution deposition studies of CdS went far beyond the solar cell field. Increasing interest in the method was due to the possibility to synthesize nanocrystalline particles. As the particle size of most solids becomes smaller than a threshold value, essential changes occur in the physical properties and crystal structure.[11] This feature is of particular importance when considering heavy-metal chalcogenides whose electronic and optical properties depend on both the particle size and structural type. The onset of quantum size effects upon reducing particle size led to introduction of the term 'quantum dots'. Unique optical properties of quantum dots, such as blue (hypsochromic) shift of the absorption edge and photoemission maximum with decreasing the quantum dot size, very bright fluorescence and photostability underlie the variety of scientific and technological applications of these systems.[12]

Colloidal semiconductor nanocrystals (colloidal quantum dots) occupy a special position. Chemically, colloidal quantum dots represent nanoparticles prepared by methods involving nucleation and growth in supersaturated solutions, *e.g.*, aqueous solution deposition. Each quantum dot is an individual mobile system stabilized by amphiphilic molecules in a solvent. The ability of quantum dots to exist in colloidal solutions allows them to be incorporated into porous organic and inorganic matrices to form composite and hybrid materials.[13–17]

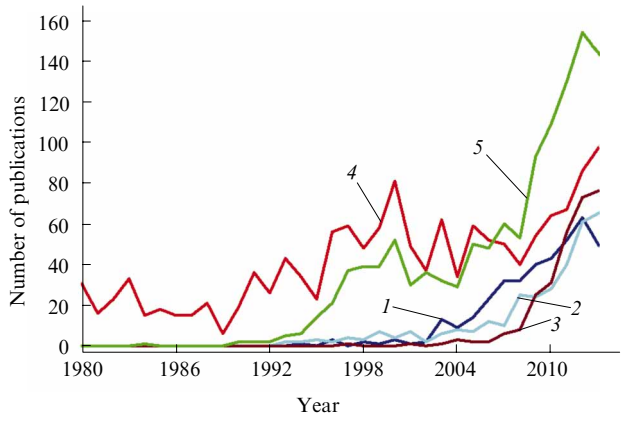


Figure 1. Distribution of publications concerning CdS over a period of 33 years (1980–2013).
Results of search based on key words: nano, bio (*1*); nano, TiO_2 (*2*); nano, TiO_2, Solar cells (*3*); Solar cells (*4*), and chemical bath deposition (*5*).

Optical properties of quantum dots based on cadmium chalcogenides make them promising for ultra-sensitive multicolour detection of biological objects, medical diagnosis, cytometry,[12,18–27] as well as in optical and electron microscopy studies and fluorescent analysis. To visualize biological objects or processes, it was proposed to embed quantum dots into the systems under study either *per se* or with 'grafted' receptors (usually, antibodies or oligonucleotides). Nanocrystals can penetrate into and distribute within targets in accordance with their properties. For instance, nanocrystals of different size penetrate biological membranes in different manner; since the fluorescence colour depends on the particle size, different regions of the target become differently coloured.[19,23,24]

The number of publications concerning biomedical applications of CdS quantum dots increased until 2012 and then began to decrease (curve *1* in Fig. 1). By that time, the ability of quantum dots to impair physiological functions of living cells was studied by toxicological, genetic, epigenetic and visual (*in vivo* and *in vitro*) methods. It was found that cadmium-containing quantum dots are potential chronic toxicants due to their physicochemical properties (particle size, surface structure, redox potential and solubility).[28] Owing to high toxicity of Cd^{2+} ions (see Refs 29 and 30) cadmium-containing nanoparticles and quantum dots cannot be treated as fully biocompatible[31] and can hardly be used in the *in vivo* studies.[32] At the same time, a study[33] in non-human primates revealed no adverse effects of CdSe/CdS/ZnS quantum dots for at least a year after administration. We believe that doubts in toxicity of CdS nanoparticles gave an impetus to search for and development of some other applications of CdS quantum dots.

Studies concerning $CdS–TiO_2$ composites make the major contribution to the overall increase in the number of publications on applications of CdS quantum dots. Until mid-2000s, main interest in this system was due to the strive for improving the properties of photocatalysts (see Fig. 1, curve *2*). The TiO_2 matrix coated with CdS quantum dots exhibits high efficiency in the visible region owing to the shift of the lower edge of the sensitivity region from 360 nm (this value is typical of TiO_2) to 510 nm.[34] The red (bathochromic) shift of the absorption edge enables photocatalytic decomposition of organics and water to produce hydrogen gas without UV irradiation.

Recent attention of researchers to $CdS–TiO_2$ composite is due to the possibility of utilizing it as a layer of quantum-dot-sensitized solar cells (see curve *3* in Fig. 1). There are convincing proofs[35] that solar-cell applications of colloidal quantum dots belong to promising and rapidly progressing investigation line in modern nanophotonics. Solar cells based on quantum dots represent third-generation photoelectric transducers that can be both more efficient and cheaper than the first- and second-generation devices based on crystalline silicon and on amorphous and polycrystalline silicon, respectively. An example of the third-generation solar cells is provided by Grätzel photoelectrochemical cells

based on a nanostructured TiO_2 or ZnO layer coated with a sensitizer (dye).[36] A particular goal in the studies of this type of solar cells is to replace [35] organic sensitizers (dyes) by semiconductor quantum dots, in particular, CdS ones.[37, 38] Chalcogenide quantum dots are basic to a novel class of solar cells, namely, quantum-dot-sensitized solar cells (QDSSCs),[37–40] because they are characterized by higher photostability and absorption coefficient compared to organic sensitizers, their band gap depends on the particle size and they are suitable for multi-exciton generation using a single photon.

In the last decade, the overall contribution of the studies on CdS quantum dots for the applications described above increased from 12% to 68% of the total number of studies on the nanostructured forms of CdS. Problems in utilizing CdS nanoparticles as quantum dots originate from some features that will be considered below. A correct description of specific structure of CdS nanoparticles (see Section II) makes it possible to clarify a complicated correlation between the properties and the particle size (see Section III). Eventually, Section IV is devoted to the preparation of CdS nanoparticles in the form of films, colloidal solutions and hybrid forms by aqueous solution deposition. In Conclusion we will outline specific features of the synthesis of various nanostructured forms of CdS and discuss the prospects for application of nanoparticles as quantum dots.

II. The structure of CdS nanoparticles: between the crystalline and amorphous states

Reducing the particle size down to the nanoscale level is accompanied by the onset of some effects that are not observed in bulk matter. First, the surface of particles now plays a significant role. At a CdS particle size of about 5 nm, the number of surface atoms is of the order of 30% of the total number of atoms in the particle. A great proportion of dangling atom–atom bonds influences the structure of the particle. As a consequence, non-crystalline structures atypical of bulk materials may appear to be more stable. For instance, close-packed metals form icosahedral clusters (periodic structures having no translational symmetry) in the nano state.[41] The structure of CdS also depends strongly on the particle size.

The α- and β-polymorphs of bulk CdS were reported for the first time by Klobukow [42] and identified as the wurtzite (*B*4 type) and sphalerite (*B*3 type) structures, respectively.[43] The notations and crystallographic parameters of the two bulk phases according to the Joint Committee on Powder Diffraction Standards (JCPDS) data are listed in Table 1. Both crystal structures are built of alternating close-packed layers, each of them being comprised of sublayers of different-type ions (Fig. 2).

The sphalerite structure is a cubic close packing with layers arranged normal to four polar directions ⟨111⟩ of the face-centred cubic (fcc) lattice. Ions within the double layer are linked by three bonds per ion, while the double layers are connected by a bond per ion. Each anion is surrounded by six same-type anions in two dimensions and by twelve same-type anions in the three-dimensional space. Cations occupy 50% of tetrahedral voids, being equidistant from four anions. Close packing of cations can be considered in a similar way.

The wurtzite structure is characterized by hexagonal close packing (hcp) with layers arranged normal to one polar direction, ⟨001⟩. The polymorphs described above are typical of bulk CdS under normal conditions; both structures are close-packed and only differ in the sequence of alternation of the packing layers on stacking. Namely, the structures can be obtained by periodically repeating the *ABC* or *AB* sequence: ...*ABCABC*... (sphalerite, see Fig. 2 *a*) or ...*ABABAB*... (wurtzite, see Fig. 2 *b*). Periodicity in the sequence of layers is a necessary condition for translational symmetry of the crystal structure.

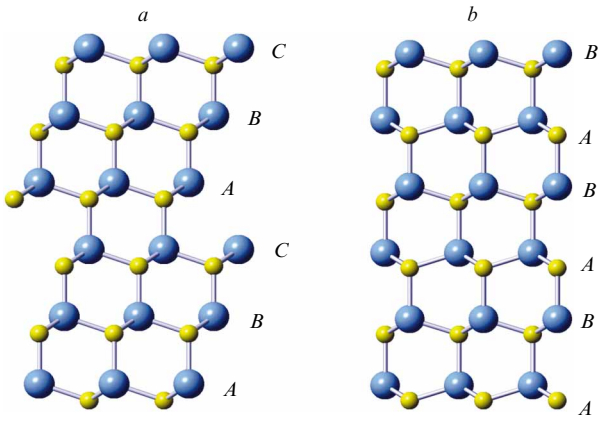


Figure 2. Crystal structure of CdS: sphalerite (*a*) and wurtzite (*b*) polymorphs.[43]

X-Ray powder diffraction analysis is most widely used for structure identification and nanoparticle size determination. Experimental X-ray diffraction patterns of films 6 to 70 nm thick synthesized by different methods,[44–52] as well as those of nanoparticles [53–55] and various complex forms of CdS [56–58] obtained using Cu $K_{\alpha 1,2}$ radiation indicate that the structures of these systems differ from those of the polymorphs of bulk CdS (wurtzite or sphalerite).

Almost all diffraction patterns of the nanostructured forms of CdS exhibit the following features: the maximum X-ray scattering intensity falls in the range $2\theta \approx 26.5–27^\circ$, two much weaker peaks being observed at $\theta \sim 44^\circ$ and $\sim 52^\circ$ (Fig. 3). In some cases, the main peak is accompanied on both sides by 'shoulders' close to the [100] and [101] reflections in the wurtzite structure. Five basic interpretations of the diffraction patterns characteristic of the nano state of CdS are as follows:

— one deals with a textured CdS film, *viz.*, there is a strong orientation along the *c* axis directed normal to the substrate surface; in this case, the phase is identified as hexagonal; [47, 48] for powders, the structure is either cubic [54, 56] or hexagonal; [52]

— a nanostructured CdS film or CdS nanopowder is a mixture of crystallites or domains of the cubic and hexagonal phases; in this case, the diffraction pattern observed is a superposition of the diffraction patterns of two phases taking into account their partial content; [44, 45, 53]

— one deals with a polytypic structure of CdS thin films; [49, 50]

— one deals with a random close packed structure of CdS nanoparticles because the sequence of layers is disordered,[59–61] the diffraction pattern corresponds to an average crystal lattice (see Table 1); and

— one deals with an amorphous nanoparticle [62] and thus with a halo in the diffraction patterns.

Table 1. Crystallographic parameters of bulk CdS phases and nanostructured forms of CdS.

Nano-particles	Structural type, mineral	PDF card number	Structure	Space group and its number	Unit cell parameters /nm		Atomic coordinates of Cd and S in the unit cell	Filling factor	CdS forms	Diffraction peaks of Cu $K_{\alpha1,2}$ radiation	
					a	*c*				2θ /deg.	*hkl*
α-CdS	wurtzite *B*4, grinockite	[JCPDS-041-1049]	hcp	$P6_3mc$ No. 186	0.414	0.672	Cd $\left(\frac{1}{3}\ \frac{2}{3}\ 0\right)$ S $\left(\frac{1}{3}\ \frac{2}{3}\ \frac{3}{\sqrt{24}}\right)$	1	powders, films, particles size > 9 nm	24.83 26.53 28.21 36.65 43.72 47.88 50.93 51.87 52.84 58.33	100 002 101 102 $2\bar{1}0$ 103 200 $2\bar{1}2$ 201 202
β-CdS	sphalerite *B*3, hawleyite	[JCPDS-042-1411]	fcc	$F\bar{4}3m$ No. 216	0.582		Cd (0 0 0) S $\left(\frac{1}{4}\ \frac{1}{4}\ \frac{1}{4}\right)$	1	microstructured films and powders	26.54 30.74 44.02 52.14	111 200 220 311
CdS 3 – 9 nm (see [b])			rcp,[a] 'average' lattice	*P*6 No. 168	0.236	0.334	Cd (0 0 0) S $\left(0\ 0\ \frac{1}{\sqrt{24}}\right)$	1/3	all forms of nano-CdS with particles 3 – 9 nm in size	~ 26.7 44.2 52.4	001 100 101
CdS < 3 nm (see [c])			amorphous	–	–	–	–	–	< 3 nm	halo ~ 27 ~ 44	

[a] Random close packing; [b] data taken from Refs 59 – 61; [c] data taken from Ref. 62.

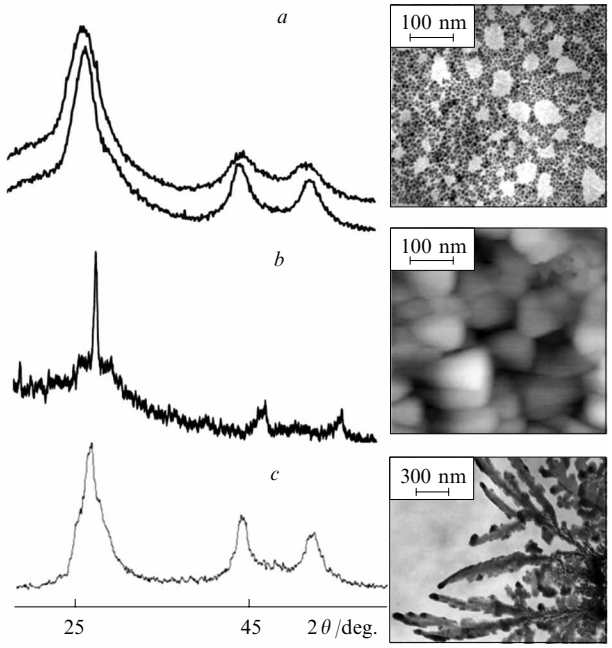


Figure 3. Different forms of nanostructured CdS: nanoparticles (*a*),[55] thin films (*b*),[51] and dendritic structures (*c*).[56] In all cases, the diffraction patterns exhibit peaks characteristic of nanostructured CdS.

The major drawback of the first two interpretations of the experimental diffraction patterns of CdS consists in the absence of some reflections typical of the wurtzite (*e.g.*, [102] and [103]) and sphalerite (*e.g.*, [200]) structures (see Table 1). Usually, this fact remains unexplained. The first interpretation requires substantiation of a particular (often, fixed) content of the crystalline phases, *B*3 and *B*4. As a rule, a correct description of the diffraction pattern by a superposition of two diffraction patterns under all synthesis conditions requires that the content of the hexagonal phase be higher ($> 60\%$). In spite of the drawbacks highlighted, the first two interpretations of the structure of CdS are most widely used.

The third interpretation considers polytypism and thus assumes various types of alternation of the sequence of layers (similarly to SiC polytypes). However, this is atypical of bulk CdS. Also, nanostructured cadmium sulfide does not exhibit new sequences of and periodicity in layer alternation; therefore, this interpretation seems to be incorrect to describe the structure of CdS nanoparticles.

The fourth interpretation takes into account the fact that the first three interpretations of the structure of CdS (either the crystal structure belonging to the *B*3 or *B*4 types or the polytypic structure) are based on a common property of atomic ordering, namely, the close packing, which is made the corner-stone. In this case, one deals with some long-range order that is responsible for strong reflections in the diffraction patterns. Contrary to this, the fifth interpretation assumes a short-range atomic order and no long-range order at all. We will consider the last two interpretations in more detail.

Specific features of the diffraction patterns of nanostructured CdS are due to disordering in the sequence of packing layers.[59–62] In this case, the probability for a layer to occupy a particular position (*A*, *B* or *C*) cannot be determined with certainty. We thus deal with a random close-packed (rcp) structure. Since the three close-packed structures of CdS, *viz.*, rcp, hcp and fcc, are characterized by identical short-range order and atomic environment and by the same number of nearest neighbours, they are rather stable from the standpoint of energy.

Structural disordering in CdS nanopowder, namely, the absence of some lines from the crystal structure in the Debye powder patterns of CdS was reported for the first time by Andrushko.[63] The structure was characterized by random superposition of anion layers and identified as intermediate between amorphous and crystal structures.

The vast majority of data point that, irrespective of the method of synthesis of CdS nanoparticles, there is a correlation between their structure and size. For instance, nanocrystalline CdS powders with an average nanoparticle size of about 5 nm have the rcp structure.[54, 64, 65] Dendritic samples[56] obtained from CdS nanopowder also consist of nanoparticles with the rcp structure characterized by a Gaussian-like particle size distribution in the range from 2 to 20 nm with a peak at 10 nm. However, large nanoparticles mainly have the wurtzite structure. In particular, spherical nanoparticles and nanofilaments 20–60 nm in size have well-defined hexagonal wurtzite structure.[66] Nanofilaments 100 nm in diameter have both hexagonal and, probably, cubic structure (nonequilibrium under normal conditions).[67]

The dependence of the structure on the particle size is also observed for CdS thin films. Based on the diffraction patterns,[49, 50, 68] the structure of a film with nanoscale domains can be identified as rcp. As the domain size in the film increases to 60 nm (see Ref. 69) and more (see Refs 70 and 71), the domain structure can be identified as wurtzite.

Structural studies of isolated particles are most labour-consuming because they require a thorough analysis of high-resolution transmission electron microscopy (HRTEM) images. For instance, HRTEM images of the rcp structure of CdS and its 'average' crystal lattice in the direct space are available.[61] Photomicrographs reported in another study[72] clearly demonstrate multiple distortions in the sequence of layers. Nevertheless, the *ABA* and *ABC* fragments were identified as wurtzite and sphalerite structures, respectively, and the overall structure was interpreted as a mixture of two phases. One or two packing defects in a nanoparticle consisting of ten close packed layers lead to the loss of translational symmetry.

Although disordered, nanostructured forms of CdS with the rcp structure remain stable at rather high temperatures. Heating of thin film samples to 720 K leads to an increase in the domain size and to a structural transition.[73] This effect was for the first time reported by Andrushko,[63] namely, it was found that the structure becomes gradually ordered above 620 K and always undergoes transition to the wurtzite structure above 820 K. In a diffraction pattern from another study[74] a clearly seen [200] wurtzite peak from bulk CdS overlaps with the peak from the major component of the film (CdS nanoparticles of unidentified structure). The maximum temperature for the synthesis of CdS with the rcp structure is 350 K. If the synthesis (or heating) is carried out at temperatures above 500 K, the CdS structure is identified as wurtzite structure which seems to be more equilibrium under these conditions. For instance, crystalline CdS nanoparticles were synthesized in a reverse micelle solution at

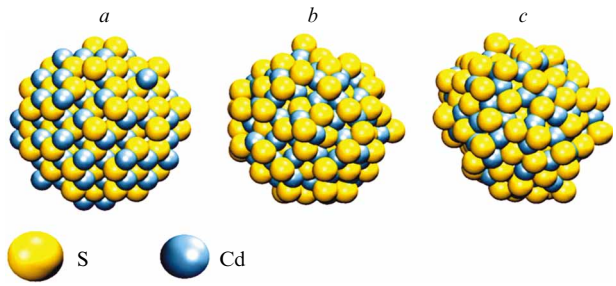


Figure 4. $Cd_{132}S_{132}$ particles of radius 1.164 nm with the sphalerite structure (*a*) after relaxation (*b*) and 'annealing' at 300 K (*c*).[62]

high temperature.[75] Micelles limit the nanoparticle size and slow down the nanoparticle growth rate, while high temperature favours atomic ordering. Nevertheless, the HRTEM image demonstrates an amorphous structure of the particle in the near-surface region. Under normal conditions, nanoparticles usually tend to form the rcp structure; here, minimization of the surface energy is due to the entropy contribution of disordering and to partial loss of translational symmetry.

The stability of structures with no translational symmetry can be assessed only using molecular dynamics (MD) calculations. For instance, *ab initio* MD calculations were used to simulate CdS nanoparticles with the wurtzite and

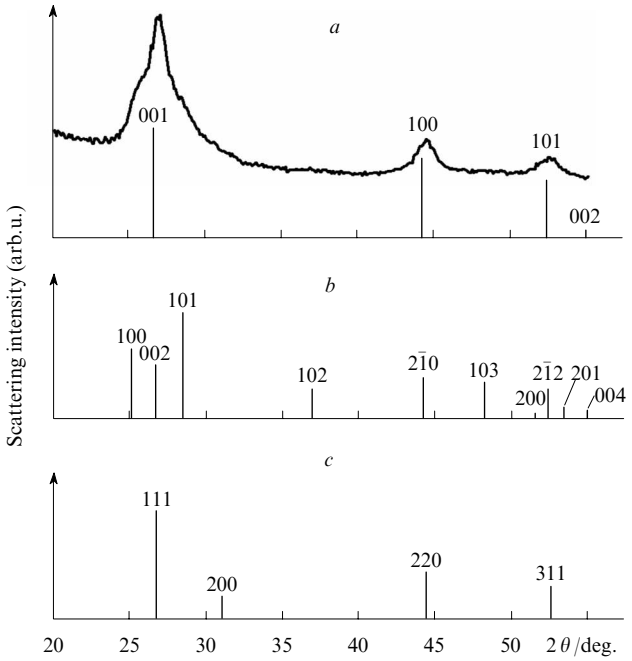


Figure 5. Experimental powder X-ray diffraction line spectra of CdS.[60]
The rcp structure, space group $P6$ (*a*); $B3$ wurtzite structure, space group $P6_3mc$ (*b*); and $B4$ sphalerite structure, space group $F\bar{4}3m$ (*c*).

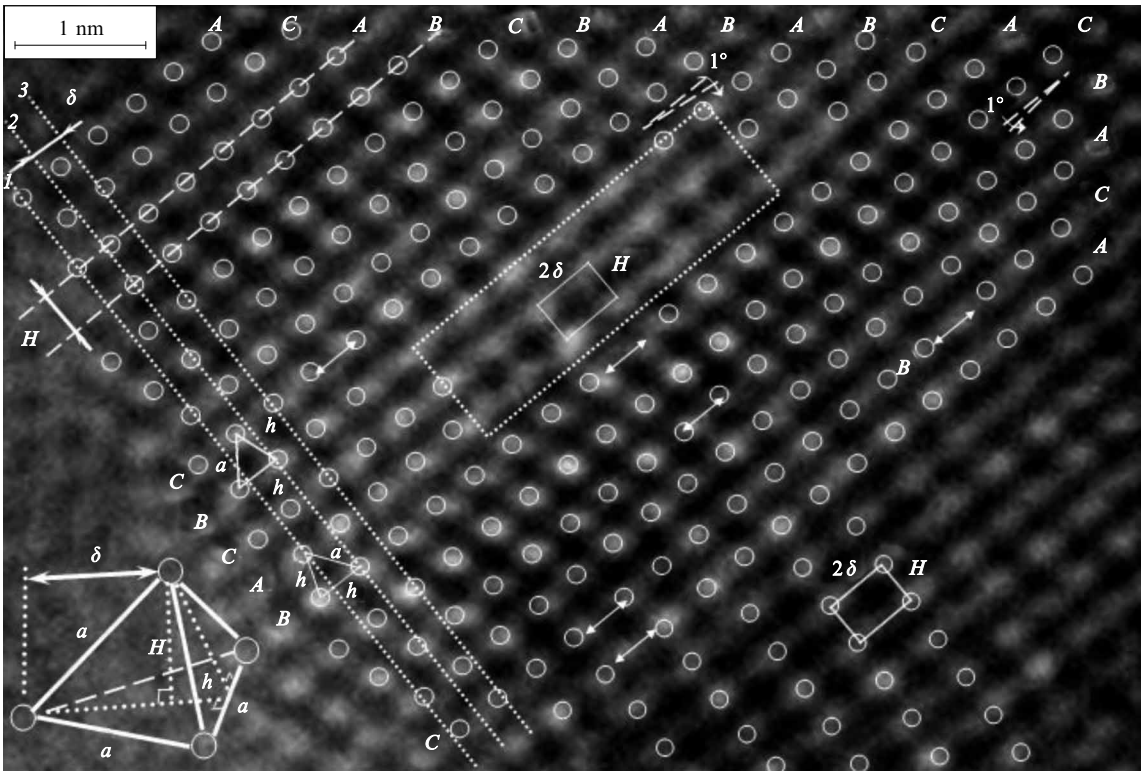


Figure 6. HRTEM image of CdS nanoparticle in the projection perpendicular to the packing layers.[61]
The circles mark the intensity maxima. A tetrahedron whose parameters a, h, H, δ correspond to the characteristic distances between the columns is shown in the lower left corner. The packing layers are arranged at an angle of 45° to the horizontal line. The layers intersecting with lines *1*, *2* and *3* are marked as *A*, *B*, and *C*, respectively. Displacements of the close-packed layers are marked by arrows. The dotted regions at the centre and in the lower right corner of the HRTEM image constitute a lattice with a rectangular unit cell $H \times 2\delta$ describing the sites of the 'average' lattice (space group $P6$) of the rcp structure of CdS.

sphalerite structures and to relax them at 300 K.[62] Using the pair distribution function of atoms in the calculated particles, it was found that the relaxed 2-nm nanoparticles lost their crystal structure and became amorphous (Fig. 4). This structure with essentially short-range order is characteristic of particles smaller than 6 nm in size.[62]

According to published data, the structure of particles 3 to 9 nm in size is characterized by an 'average' long-range order,[59–61] which manifests itself as well-defined peaks in the diffraction patterns (Fig. 5). Namely, scattering by randomly alternating packing layers leads to the loss of information on periodicity in the sequence of layers. Only information that atoms belong to layers that can occupy any of the three positions (*A*, *B* or *C*) remains valuable; this is equivalent to the statement that the packing layer equiprobably occupies all three positions (occupation probability is 1/3). Therefore, the rcp structure was associated with a hexagonal lattice, space group $P6$ (C_6^1) and the unit cell parameters $a = 0.236$ and $c = 0.334$ nm, where a is the distance between the projections of all atoms on the packing plane and c is the distance between the nearest close-packed layers of same-type atoms (Cd or S).[60,61] In the unit cell of the 'average' lattice, Cd and S atoms occupy single positions 1(*a*), the atomic coordinates and the filling factors are listed in Table 1.[76]

The 'average' lattice is primarily needed to explain the results of the X-ray diffraction study and characterizes a statistical probability of a position rather than actual atomic arrangement in the particle. Actual atomic positions in the amorphous structure can be seen in the HRTEM image of a CdS particle (Fig. 6), in particular, atomic columns and close-packed layers; atomic columns consist of Cd atoms characterized by high electron scattering factor. The complete sequence of packing layers in the HRTEM image is aperiodic and can be written as *ACABCBABABCACBACA*. A thorough analysis of the HRTEM image makes it possible to identify features in the dashed area as image of the 'average' crystal lattice (space group $P6$) of the rcp structure of CdS. Visualization of this lattice in Fig. 6 is due to the superposition of one-dimensional projections of the layers *A*, *B* and *C*. The interatomic distance determined from the HRTEM image is 0.41 ± 0.01 nm.

Summing up, the structure of nanostructured forms of CdS depends strongly on the particle size. There are two critical sizes. If a particle consists of a few thousands of atoms, tetrahedral environment of Cd and S atoms leads to formation of packing layers and to 'average' long-range order. This structure is characteristic of CdS particles whose size is between 3 and 9 nm. Particles comprised of a few hundreds of atoms have a size of about 2 nm and amorphous structure. Unambiguous determination of the particle size corresponding to the boundary between amorphous particles and particles with the rcp structure is impossible; therefore, we will use a value of 3 nm as the upper bound of the size for the particles with amorphous structure.

III. Properties of CdS nanoparticles: the size and surface effects

As the size of a semiconductor crystal decreases to nanoscale level in one, two or three dimensions, the electronic structure and properties of the material change essentially.[77] Discrete structure of the electronic energy levels in semiconductor nanoparticles allows them to be considered as 'artificial atoms'. Early in the 1980s, researchers from the USSR predicted and then discovered the blue shift of the absorption edge upon size reduction of CdS nanoparticles.[78,79] This also implies the possibility of controlling other properties, in particular, luminescence. However, changes in the electronic, magnetic, optical and other properties with decreasing particle size are due to the influence of two factors including the size confinement effect and an increase in the surface-area-to-volume ratio. In this Section, we will consider how these factors affect the properties of nanoparticles in order to demonstrate the possibility of synthesis of quantum dots based on CdS nanoparticles.

III.1. Optical absorption

For CdS nanoparticles (1.5 to 40 nm in size) dispersed in a dielectric glassy matrix, the blue shift increased with decreasing particle size and reached a value of 0.8 eV at the minimum size.[78] According to the first theoretical model,[79] the band gap increases due to quantization of states of an exciton in the potential well with infinitely high walls (the potential well boundaries are specified by the surface of the spherical semiconductor particle). Quantization due to spatial confinement manifests itself for particles whose size is comparable or smaller than the diameter of an exciton (5.8 nm for CdS). In this case, the absorption edge is given by

$$E = E_g + \frac{0.71\pi^2\hbar^2}{2\mu r^2}$$

where E_g is the band gap in the bulk crystal;

$$\mu = [(m_e^*)^{-1} + (m_h^*)^{-1}]^{-1}$$

is the reduced mass of exciton (for CdS, one has $m_e^* = 0.2\,m_e$ for the effective mass of electron, $m_h^* = 0.81\,m_e$ for the effective mass of hole and $m_e = 9.1 \times 10^{-31}$ kg or the rest mas of electron) and r is the radius of the particle. A more detailed expression for the dependence of the exciton energy on the nanoparticle size has the form

$$E = E_g - 0.248E_{Ry} + \frac{n^2\pi^2\hbar^2}{2\,\mu r^2} - \frac{1.786\,e^2}{\varepsilon r} \quad (1)$$

where

$$E_{Ry} = \frac{\mu e^4}{2\,n^2\hbar^2}$$

is the effective Rydberg energy (electron–hole binding energy), n is a non-negative integer, e is the charge of an electron and ε is the dielectric constant of the particle.[80] The sum of the first three terms equals the exciton energy in a macroscopic crystal, while the fourth term includes the Coulomb interaction between electron and hole. Having experimentally determined the band gap, one can estimate the average particle radius:

$$r = 2\pi\hbar(8\mu\Delta E_g)^{-1/2}$$

This expression is suitable for calculation of the particle diameter (D/nm) from the experimentally determined blue shift (in eV),

$$D = \frac{3.062}{\sqrt{\Delta E_g}}$$

Since the blue shift of absorption edge belongs to the quantum size effects, CdS nanoparticles can rightly be called quantum dots.

Linearized muffin-tin orbital (LMTO) calculations[81,82] of the density of electronic states in CdS nanoclusters showed that the band gap in CdS nanoparticles increases owing to the shift of the bottom of the conduction band (BCB) towards higher energies and shift of the top of the valence band (TVB) towards lower energies. Experimental confirmation of the shift of the TVB and BCB in thiol-stabilized CdS nanoparticles with decreasing particle size was obtained in a soft X-ray spectroscopy (SXS) study.[83] It was shown that two effects contribute to the increase in the band gap. These are narrowing of the valence band from 4.7 to 3.5 eV and separation in the conduction band of contributions from the size confinement effect of excitons and from quantization of the density of states in the conduction band.

The best fit of the dependence of the band gap on the particle size is given by[81,82]

$$\Delta E_g = 2.83\,e^{-D/8.22} + 1.96\,e^{-D/18.07} \quad (2)$$

or

$$\Delta E_g = \frac{36.9}{D^{1.2}} + \frac{269.7}{D^{2.2}} \quad (3)$$

where D is the nanoparticle diameter in Å and ΔE_g is in eV. Both expressions describe the decrease in the shift of the absorption edge with increasing crystal size (Fig. 7).[79–85] The best correlation with experimental data was obtained in calculations within the framework of the effective mass approximation for an exciton in a potential well of finite depth.[84]

III.2. Phonon spectra

Similarly to electrons and holes, phonons also experience the size confinement effect in nanocrystals. In bulk crystals, the proper state of a phonon is a plane wave, and the selection rules of the wave vector q for the first-order Raman scattering require that $q \approx 0$. This rule violates in the case of finite spatial function of the phonon (its confinement to the size of the nanoparticle). Localization of optical phonons leads to a red shift of the Raman scattering frequencies of longitudinal optical (LO) phonons[86–88] from 304.5 to 297–302 cm^{-1}. Assuming a spherical shape of small quantum dots, the wave vector is

$$q = \frac{\pi m}{D}$$

where m is the quantum number of the localized mode and D is the diameter of the quantum dot. Dispersion $\omega(q)$ of LO phonons in CdS is negative; therefore, the frequency of the first localized mode (LO_1) appears to be lower than the corresponding bulk value. The scattering frequency of LO phonons is plotted *vs.* nanoparticle size in Fig. 8.

In the frequency range between the bulk longitudinal optical (ω_{LO}) and transverse (ω_{TO}) phonons the dielectric constant of the crystal $\varepsilon(\omega)$ is negative and, correspondingly, the wave vector values

$$k = \frac{\omega}{c}\sqrt{\varepsilon(\omega)}$$

(ω is the phonon frequency and c is the speed of light) are imaginary. Because of this, waves in bulk crystals cannot exist in this frequency range; only the surface modes (ω_{SO}) are allowed.[89] The experimental and calculated frequencies of SO-modes obtained taking into account localization of optical phonons are 245,[86] 272,[87] 280 (see Ref. 89) and 290 cm^{-1}.[90] The scatter of the experimental and theoretically determined values is due to strong influence of electron–phonon coupling.[87] No dependence of the SO-modes on the size and shape of CdS nanoparticles was reported.[90]

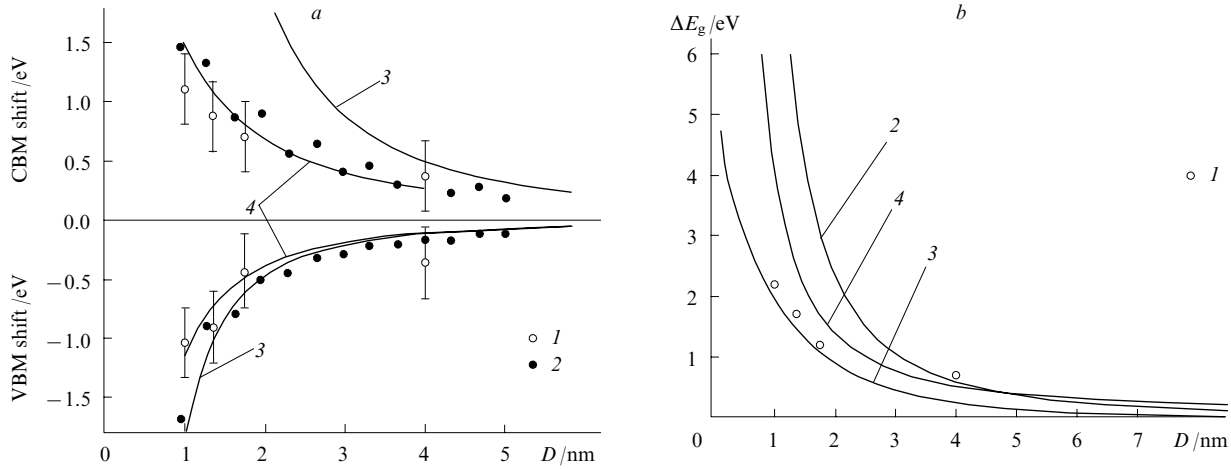


Figure 7. Calculated and experimental dependences of changes in the band gap on the CdS particle size.
(*a*) Shift of the valence band maximum (VBM) and conduction band minimum (CBM); experiment (*1*),[83] published data[85,79,84] (calculations) (*2–4*); (*b*) changes in the band gap; experiment (*1*),[83] calculations: (*2*) from Eqn (1),[79,80] (*3*) from Eqn (2),[81] *4* from Eqn (3).[82]

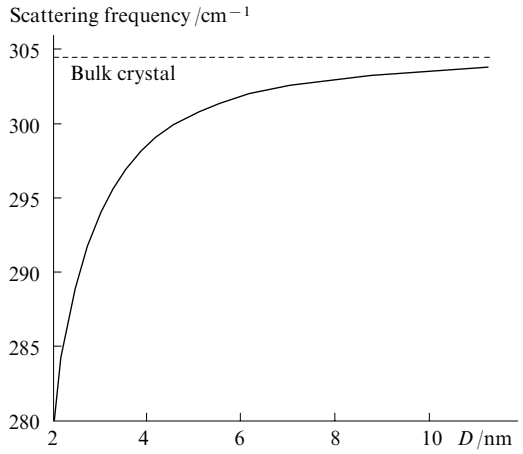


Figure 8. Scattering frequency of longitudinal optical LO-phonons plotted *vs.* CdS nanoparticle size.[87]

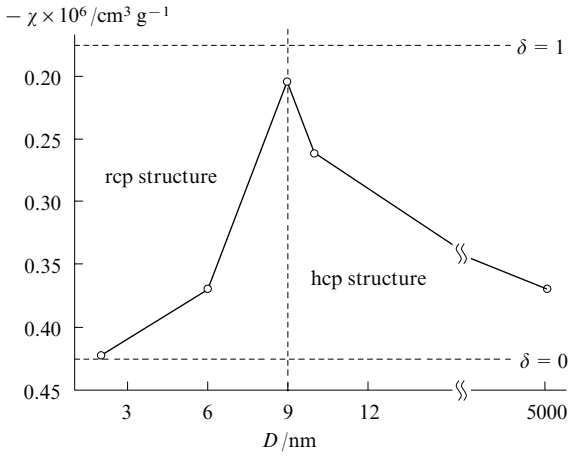


Figure 9. Magnetic susceptibility of CdS plotted *vs.* particle size.[93] δ is the bond covalency.

By and large, the phonon properties of CdS illustrate the importance of the quantum size effects and surface effects. The former leads to the size confinement effect of optical phonons, while the latter is responsible for the formation of the surface modes. Although these effects are in fact mutually independent, it is clear that the proportion of surface atoms depends on the particle size; however, this can be better understood by analyzing the dependence of the magnetic susceptibility on the particle size.

III.3. Magnetic susceptibility

The magnetic susceptibility belongs to a small group of the properties of matter that are determined by the electronic subsystem only, being independent of the energy spectrum of phonons. By analyzing the behaviour of the magnetic susceptibility of nanoparticles one can more correctly separate the influence of the particle size and particle surface on the electronic properties. An increase in the magnetic susceptibility of CdS upon reduction of the particle size to 100 nm was for the first time reported Aresti *et al.*,[91] who attributed this effect to the increase in the proportion of surface atoms with dangling bonds. The magnetic susceptibility (χ) of undoped semiconductor is determined by the Langevin diamagnetism of electrons in the closed shells of ion cores (χ_c), by diamagnetism of valence electrons (χ_v); in the case of $A^{II}B^{VI}$ semiconductors, one should take into account the van Vleck paramagnetism (χ_p) of distorted electron clouds of the sp^3 orbitals.[92] All these things being considered, the magnetic susceptibility is given by

$$\chi = \chi_c + \chi_v + \chi_p$$

For CdS, the magnetic susceptibility can be determined from the expression

$$\chi = (-0.426 + 0.249\,\delta) \times 10^{-6}\ \text{cm}^3\ \text{g}^{-1}$$

where δ is the bond covalency or the shape asphericity of the sp^3-electron cloud.

Estimation of the van Vleck paramagnetism contribution[93] showed that a decrease in the size of wurtzite CdS nanoparticles causes the bond covalency to increase and reach the limiting value for extended wurtzite particles with an average size of 9 nm (Fig. 9). Particles smaller than 9 nm in size have the rcp structure and the shape asphericity of the sp^3 orbitals abruptly decreases to a value typical of bulk CdS. The sp^3 orbitals of 2-nm amorphous particles have almost undistorted shape and the atom–atom bonds can be treated as ionic. The reason for such a behaviour of the magnetic susceptibility consists in that for the hexagonal or cubic packing, the surface-area-to-volume ratio sharply increases as the particle size decreases (<9 nm). To reduce the number of dangling bonds, one should change the environment of the surface atoms, which can be done if the sequence of alternation of the close-packed layers is violated and the rcp structure is formed.

High shape asphericity of the sp^3 orbitals in crystalline particles is confirmed by the temperature induced magnetic susceptibility drop followed by changes in the shape of nanoparticles owing to surface changes. Thermally induced excitation of the surface causes its structure to break down; it can be changed *via* growth of the particle or redistribution of the surface atoms. The temperature of the magnetic susceptibility drop for >9-nm wurtzite particles was 250 °C (*cf.* 310 °C for smaller particles with the rcp structure). The effect was confirmed[94] by differential scanning calorimetry (DSC) data for 8-nm nanoparticles. The DSC traces of both freshly synthesized and aged samples exhibit an exothermic peak in the region 281 °C, the rcp structure and the shape of nanoparticles remain unchanged to 300 °C, thus indicating that thermal effects only influence the surface of particles. At higher temperatures, the particle size increases owing to lateral growth of packing layers rather than formation of new close-packed layers. Quantum chemical calculations[95] of the stability of 2-nm CdS clusters predict an increase in the proportion of surface atoms and a decrease in the proportion of bulk atoms on heating above 130 °C and irreversible structural changes above 300 °C.

Summing up, the phonon spectra and magnetic susceptibility depend not only on the particle size, but first of all on the proportion of surface atoms, which increases as the particle size decreases. The state of the surface governs the internal structure of nanoparticles, namely, if the particle size is smaller than 9 nm, the rcp structure appears to be more stable than the hcp structure.

III.4. Photoluminescence

The blue shift of the optical absorption edge with decreasing nanoparticle size implies a corresponding blue shift of the luminescence band. The latter effect is of importance for practical applications of quantum dots as luminophores or biomarkers. Seemingly, calculations predict a band gap of 3.5 eV for 2-nm CdS nanoparticles (see Fig. 7 *b*); correspondingly, luminescence should occur in the UV region at 350 nm. However, in most studies the blue shift of luminescence is not observed, or does not reach the characteristic values, or one deals with a red shift relative to the peak at 510 nm characteristic of bulk cadmium sulfide.

Probably, disagreement between the absorption and luminescence bands is due to structural disorder. However, a large shift of luminescence maximum to 725 nm was observed in the case of highly crystalline particles 3–6 nm in size synthesized in reverse micelles.[96] Correspondingly, the red shift cannot be attributed to low degree of crystallinity of particles. On the contrary, such a large red shift indicates that perfect crystal structure of CdS nanoparticles leads to numerous defect surface states. Amorphization of the surface of particles synthesized in reverse micelles was also reported in another study.[73]

Theoretically, the red shift of luminescence maximum relative to the absorption edge was described for solid solutions of cadmium chalcogenides in which quantum dots are formed by the vacancy clusters.[97] According to calculations, the influence of different types of electron–phonon coupling causes additional, oppositely directed Stokes shifts of the absorption and luminescence bands.

As mentioned above, disordering in the sequence of layers is accompanied by a decrease in the number of dangling bonds and the red shift should thus decrease. Particles whose structure is characterized by twinning[88] (this allows the structure to be identified as rcp) luminesce at 550 nm. Glutathione-passivated cadmium sulfide nanoclusters $Cd_1S_{0.47}GS_{0.53} \cdot 2.5\,H_2O$ with the CdS core 1.3 nm in diameter and a shell 0.5 nm thick exhibit a blue shift of the absorption band and a shift of the luminescence band at 550 nm.[98] Similar changes in the photoluminescence and optical absorption are also characteristic of thin films prepared by aqueous solution deposition.[99] The band gap in the films annealed at 450 °C decreased from 3.50 to 3.46 eV, while the particle size increased from 2.60 to 2.64 nm. Annealing was followed by a red shift of the luminescence maximum from 520 to 544 nm, which was associated with an increase in the number of surface defect states in the sulfur sublattice.

Theoretical calculations[100] of the behaviour of the surface sulfur atoms at the cleavage of a CdS crystal revealed small atomic displacements relative to the upper layer of cadmium atoms and showed that the smaller the number of bonds between the atom and the surface the larger the displacement. These displacements of sulfur atoms on the surface of crystals lead to formation of clearly seen surface states at the top of the valence band. Calculations[81] revealed strong influence of dangling bonds on the energy band structure. Numerous unoccupied orbitals may give rise to electronic states in the band gap on the particle surface. In the case of photoluminescence, these states can act a electron traps and, consequently, induce a red shift. After improvement of the models, namely, elimination of unoccupied surface orbitals in the model particles (this is analogous to passivation of the surface), the states within the band gap disappeared.

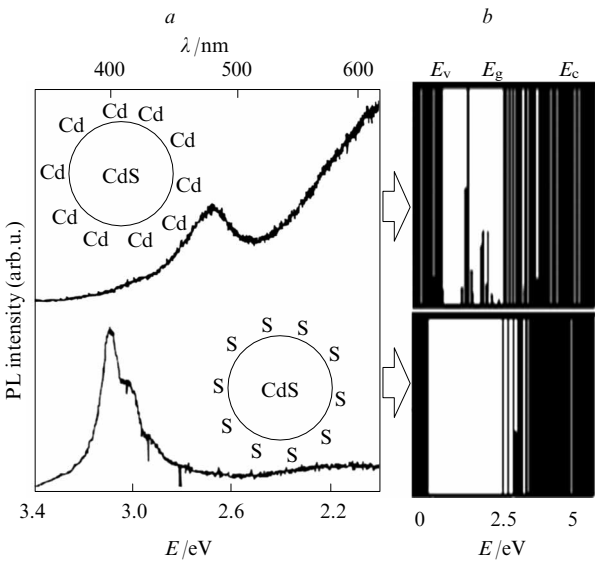


Figure 10. Blue shift of photoluminescence (PL) of CdS quantum dots due to suppression of defect states in the band gap by passivation of the surface of CdS nanoparticles.
Experiment (*a*)[101] and energy band structure calculations (*b*).[81]

The influence of passivation of the surface layer on the luminescence of CdS nanoparticles was confirmed experimentally.[101] The surface sulfur layer was removed by etching the surface of particles with hydrochloric acid and the Cd : S ratio became as high as 3 : 1. In the presence of excess cadmium the proportion of defect surface states increased and a red shift of the luminescence peak was observed. If the surface of nanoparticles was passivated with a sulfur shell 3 nm thick, a blue shift of the luminescence peak was observed (the smaller the particle size the larger the shift, see Fig. 10). If no passivation of the surface of CdS nanoparticles occurred, a chemical analysis revealed the presence of excess cadmium, namely, a Cd : S ratio of 1.1 : 1 (see Ref. 65) or 1.0 : 0.72 (see Ref. 69).

Thus, the red shift or, more exactly, the absence of the expected blue shift, is due to the formation of surface trap states in the band gap and to electron–phonon coupling. To induce a blue shift, one should suppress the formation of surface trap states in the band gap of CdS quantum dots.

The most widely used and efficient method for elimination of surface states is to passivate the nanoparticle surface with an organic or inorganic shell surrounding the CdS core. At the same time, coating a nanoparticle with an organic shell may give rise to luminescence maxima in the red and infrared regions. For instance, luminescence of CdS nanoparticles surrounded by oleic acid molecules is characterized by three broad peaks in the region from 515 to 1030 nm. A maximum at 704 nm (1.76 eV) is produced by the surface defect states characteristic of crystalline nanoparticles. Two maxima at 576 nm (2.15 eV) and 905 nm (1.72 eV) are a result of the influence of the bonds between the surface atoms of the nanoparticle with the organic shell.[102]

Yet another successful method for suppression of surface states in the synthesis of nanoparticles from aqueous solutions is to combine irradiation and an increase in the

pH value of the solution.[103] An increase in the pH value stimulates desorption of thiol molecules and the formation of Cd–OH bond (at pH 11), which leads to elimination of the surface defect trap states and, as a consequence, ensures an increase in the photoluminescence intensity. Irradiation with visible light can be utilized for the etching of nanoparticles to induce a blue shift of the luminescence band; the shorter the wavelength the larger the blue shift. By varying the illumination conditions and the concentration of H^+ ions near the surface of the particle one can control the particle growth.[104]

The blue shift of the luminescence peak from 515 to 420 nm in the synthesis of 1.5-nm nanoparticles in a matrix is accompanied by substantial broadening of the peak owing to the influence of defect states at the quantum dot/matrix interface.[105] The intensity of luminescence of 5-nm nanoparticles characterized by the peak at 420 nm (2.95 eV) appreciably increases upon passivation of their surface in various solutions.[64] For the 8-nm nanoparticles synthesized in reverse micelles, the blue shift and narrowing of the luminescence peak from 550 to 410 nm originate from 10-min reflux (removal of water from micelles).[57] Nanoparticles 1.5–1.8-nm in size deposited from DMSO solution and having the rcp structure are characterized by a luminescence peak at 460 nm (2.7 eV).[106]

The photoluminescence intensity maximum in the region of 420 nm (2.95 eV) can be interpreted in different manner. On the one hand, one deals with the blue shift relative to the luminescence peak at 510 nm (2.42 eV) of bulk CdS. On the other hand, such a behaviour of the luminescence of nanoparticles < 4 nm in size can be treated as red shift compared to the absorption edge shift and to an increase in the band gap by more than 0.5 eV. By and large, the photoemission wavelength depends slightly on the particle size, being to a greater extent influenced by the surface passivation technique.

Weak blue shift of photoluminescence is usually explained by nonradiative recombination of excitons from the remaining surface trap states. The exciton energy is 3–5 eV depending on the quantum dot size. However, recombination of an exciton involves energy consumption in nonradiative processes and through emission from the surface trap states. This is possible if charged excitons (trions, biexcitons and multi-excitons) are formed. A trion is formed from an exciton and a charge carrier and can be charged either positively (T^+) or negatively (T^-). The T^+ trion is composed of two holes and an electron, while the T^- trion comprises two electrons and a hole; the like charges in the trion have oppositely directed spins. Diexcitons and multi-excitons are composed of bound electron–hole pairs. Recombination of a single exciton can produce only a photon with the corresponding energy, whereas recombination of a trion state involves energy transfer to the remnant charge carrier and subsequent redistribution of this energy through different channels. For instance, decomposition of the T^- trion may be followed by transition of the remnant electron to higher-energy states in the conduction band, or decomposition of the T^+ trion may be followed by trapping the remnant hole or by the remnant hole transition to deeper-lying states in the valence band. The remaining energy can be consumed through emission of a photon, including photon emission on transitions of the charge carrier between traps in the band gap. Analogously, recombination of an exciton within diexcitons and multi-excitons may be followed by energy redistribution through different channels.

Thus, the synthesis of quantum dots with specified luminescent properties should be carried out taking into account both the influence of the surface trap states and nonradiative Auger processes. Efros, one of the authors of a pioneering study [79] in which blue shift in CdS nanoparticles was predicted, wrote in 2009: 'In the early sixties, the one-dimensional carrier confinement achieved in semiconductor quantum wells and superlattices brought about a revolution in solid-state device technology... However, the application of nanostructures to real-world devices has been strongly curtailed by the enhancement of dissipative Auger processes that undergird all aspects of carrier relaxation and recombination. In particular, Auger processes have been attributed to the decrease of the photoluminescence quantum efficiency, photoluminescence degradation and photoluminescence blinking in nanocrystal quantum dots'.[107]

Auger processes in nanoparticles were ignored for long because the probability for such processes to occur in bulk crystals is negligible. Permanent irradiation of nanoparticles is accompanied by random charge–discharge processes. Absorption of a photon or creation of an electron–hole pair followed by emission of a photon do not influence electrical neutrality of nanoparticles. But if a nanoparticle bears an excess charge, a trion state is formed and nonradiative Auger recombination occurs. The rate of Auger recombination is a few orders of magnitude higher than that of radiative exciton recombination; correspondingly, this process is much more probable. Also, Auger processes involving surface trap states can occur.[108]

It was predicted theoretically [107] that high efficiency of Auger processes is due to abrupt termination of the electron potential at the particle boundaries or heterointerfaces. Electron and hole tend to localize at the quantum dot boundaries; in the case of a charged nanoparticle and formation of a trion state, this provokes the remnant charge carrier to delocalize from the core and to form a surface state.[109] Methods to avoid this process are different for different trion states (T^- and T^+).

If the T^- trion is formed, it is necessary that both electrons be on the same energy level. At $T < 200$ K, a 100% quantum yield of luminescence in CdSe@CdS core–shell quantum dots can be attained.[109, 110] At the same time, experiments showed that the rate of Auger recombination of the T^- trion in CdS nanoparticles increases by three orders of magnitude (from 2.2 ns to 57 ps) as the particle size decreases from 3.2 to 1.4 nm.[111]

The decomposition rate of T^+ trion is a few orders of magnitude lower, but the probability of formation of this state is also much lower. According to calculations,[107] Auger processes accompanying recombination of T^+ trions can be suppressed in a soft potential. In Fig. 11 the rate ($1/\tau_A$) of Auger processes accompanying the decomposition of T^+ trion in nanoparticles is plotted *vs.* particle size. These results were obtained from calculations with different-shape potentials. As can be seen, in the soft potential the larger the particle size the slower Auger processes. In this case, the quantum yield of luminescence in 10-nm CdSe/CdS chalcogenide particles can be as high as 90% at room temperature.[110]

Uncoated CdS nanoparticles are characterized by abruptly terminating potential boundaries. In this case, the Auger processes can be suppressed for so-called magic-size

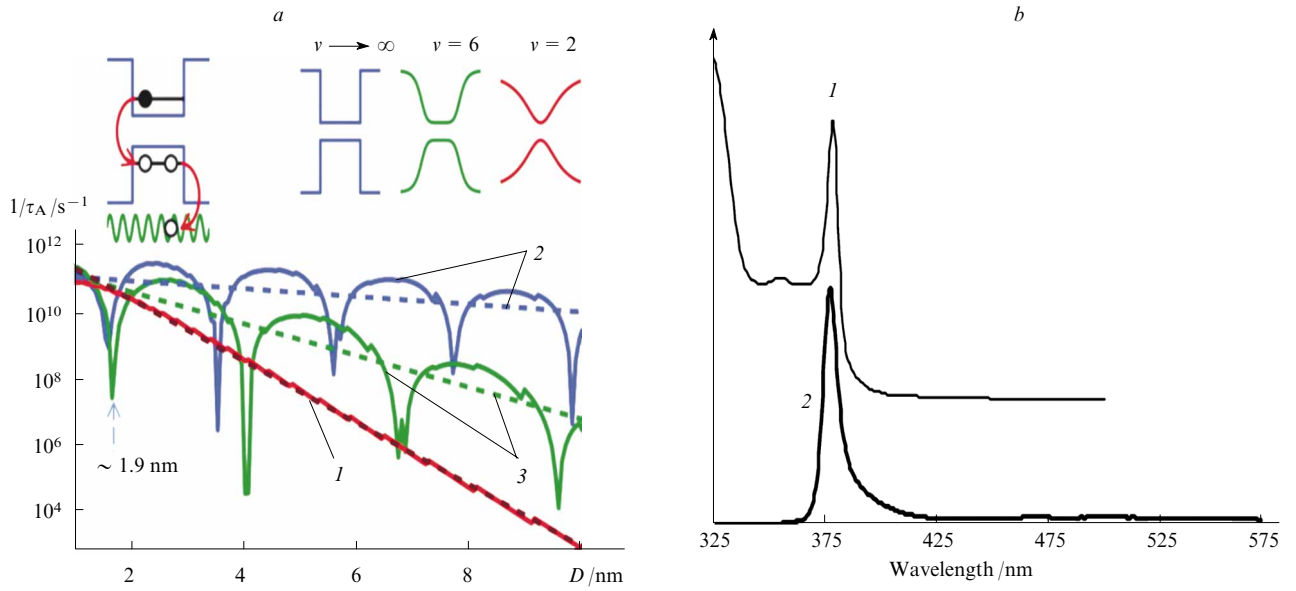


Figure 11. Rate of Auger processes accompanying decomposition of T^+ trion (schematically shown in the upper left corner) plotted *vs.* particle size for different types of confinement (*a*) and the luminescence spectra and optical absorption spectra of monodisperse CdS nanoparticles with a magic size of 1.9 nm (*b*).[112]
(*a*) For soft potential, the rate of Auger processes increases as the particle size decreases (line *1*), for potentials with abruptly terminating boundaries, (curves *2* and *3*), the Auger processes are suppressed for the magic-size particles;[107]
(*b*) absorption (*1*) and emission (*2*).

particles. For instance, the decomposition rate of T^+ trion in ~1.9-nm particles can be decreased by a few orders of magnitude using different-shape potentials characterized by the parameter *v*. Probably, this effect was confirmed in a study [112] where 1.9-nm CdS nanoparticles synthesized *via* one-pot noninjection approach demonstrated a well-defined blue shift of the absorption edge and photoluminescence peak to 378 nm (3.28 eV). Ligands formed strong bonds with the nanoparticle surface. According to NMR spectroscopy data, the surface cadmium atoms were bonded to both COO groups and sulfur atoms, whereas bulk Cd atoms were only bonded to sulfur atoms. The quantum yield was about 10%. One can assume that luminescence in these particles is induced by exciton recombination that is due to suppression of Auger processes (recombination of T^+ trions) in the magic-size nanoparticles rather than elimination of surface traps.

Summing up, the properties of CdS nanoparticles depend strongly on their size and on the proportion of surface bonds. A correct theoretical description of the blue shift of absorption edge, the red shift in the spectra of longitudinal optical phonons and the formation of surface modes with decreasing particle size is available. The results of calculations agree with experimental data. The luminescent properties of CdS nanoparticles depend on the particle size, structure and surface in a complex manner.

IV. Aqueous solution deposition of nanostructured forms of CdS: from thin films to colloidal systems

Chemical bath deposition (CBD), or chemical solution deposition (CSD), or simply chemical deposition (CD) is a well-known method. For instance, back in 1835 Liebig [113] used it to deposit silver on the rear surface of a piece of glass. The first publication on the chemical deposition of semiconductor films was appeared in 1869;[114] it concerned preparation of coloured PbS, Cu_xS and Sb_xS_y films from aqueous thiosulfate solutions of lead acetate, copper sulfate and antimony tartrate. Since then, the method has been used to prepare thin-film semiconductor materials. Chemical bath deposition is the simplest method for the synthesis of such materials. Carrying out a CBD study requires a reaction vessel (usually, a glass vessel), the starting reactants are cheap and readily available, mixers and thermostats are only useful options; in other words, there is no need for complex expensive equipment, heating to high temperatures or toxic and explosive reactants.

The first classification of physical and chemical deposition methods was reported by Chopra and Das,[115] who showed that chemical bath deposition can be considered as an ultimately formed and promising method. This publication was followed by Lokhande's review [116] of the compositions of the reaction mixtures for the synthesis of chalcogenides developed before 1991. Lincot and co-workers were the first who generalized the available information on the homogeneous and heterogeneous nucleation, on the mechanism and kinetics of formation of binary and ternary sulfide, selenide and telluride films by chemical bath deposition.[117] Particular data on the mechanisms of CdS and ZnS film deposition and on the use of thermodynamic constants to describe the initial composition of the reaction mixture were reported [118] a year before Lincot. Tradition to use the principles of chemical thermodynamics and chemical kinetics in order to choose the composition of the reaction mixture and to describe the mechanisms of reactions occurring in the course of chemical bath deposition (for more detail, see below) was rooted in the 1960s and consolidated in the 1990s.[2–5,115–118] The next group of reviews concerned the results obtained in a research group from India,[119] in studies of chemical bath deposition of

semiconductors for thin-film solar cells.[120] The potential of the title method was studied in connection with the synthesis of not only metal chalcogenides,[121] but also oxides[122–125] and ceramic materials.[126] In 2007, the first review concerning applications of CBD to preparation of nanocrystalline semiconductor films was reported.[127] Cadmium sulfide films were for the first time prepared from solutions by Mokrushin and Tkachev in 1961.[2] These films as well as other sulfide films are deposited using various sources of sulfide ions (see Section III.2).

In spite of experimental simplicity, in-depth investigation of the mechanisms of deposition of solids, which is necessary to extend the possibilities of controlling the composition and various properties of compounds formed, is a stubborn problem. In this connection, we believe that the method of chemical bath deposition is still not of common use.

Chemical bath deposition as simple, cheap and industrially convenient method for preparation of just thin films on metallic, semiconductor and insulating substrates has been a subject of numerous reviews.[115–127] As important advantage of the method consists in low rate of chemical reactions, which makes it possible to synthesize well-crystallized particles for deposition of films with specified texture. Interestingly, each research group has its own ideas of the mechanisms of thin film formation on substrates.

In this review, we for the first time consider chemical bath deposition as promising method for preparation of not only bulk thin-film structures, but also nanostructured semiconductor particles of different structure taking CdS as an example. Among the physical and chemical deposition methods, only chemical bath deposition yields various bulk and nanocrystalline hybrid forms of semiconductor compounds including CdS not only as continuous or island-type films on surfaces of any size and configuration, but also as core–shell structures, agglomerated polycrystals of regular shape and isolated particles in colloidal solutions.

IV.1. Aqueous solution deposition: theoretical aspects

Traditionally, a reaction mixture for CBD represents a solution of one or more salts of the metal M^{n+}, a source of chalcogen X (X = S, Se, Te) and a complex-forming agent. Metal chalcogenide deposition involves the following four steps:[125]

1) formation of equilibrium homogeneous system complex-forming agent–water;

2) formation and dissociation of a complex metal compound $[ML_i]^{n+ik}$, where L denotes one or more ligands, n is the oxidation state of the metal M, i is the number of ligands and k is the charge of the ligand;

3) hydrolysis of the source of chalcogen; and

4) formation of solid metal chalcogenide.

A feature (often, a drawback) of the synthesis in aqueous solutions is the possibility for side reactions resulting in almost water-insoluble oxygen-containing metal compounds to accompany the main reaction affording inorganic chalcogenide (stage 4). The formation probability of side products is rather high because most metal ions are hydrolyzed in aqueous solutions. Hydrolysis significantly complicates the synthesis of pure compounds containing no basic salts and hydroxides. In this connection, a particular complex-forming agent for each metal ion should be used in stage 2 in order to suppress hydrolysis and to control the feed rate of metal ions to the reaction zone in stage 4.

Stage 3 is accompanied by a decrease in the concentration of metal cations due to the appearance of chalcogen ions X^{m-} in the solution and formation of solid chalcogenide M_mX_n. Stage 4 is an almost irreversible reaction. Aqueous solution deposition is carried out in a closed system at constant temperature (T) and pressure (p). In this case, irreversible changes are always accompanied by a decrease in the Gibbs free energy (ΔG).[58] For processes conducted at constant temperature and pressure, the Gibbs free energy is an indicator of irreversibility. However, the system where a metal chalcogenide is formed, is in partial equilibrium. According to Prigogine, the system is in partial equilibrium if it is in mechanical and thermal equilibrium, but there is no equilibrium with respect to the distribution of matter between the components that can interact chemically, with respect to the distribution of matter between different phases of the system and, generally, with respect to any changes that can be characterized by the reaction coordinate ξ.[128] Consider a system where the ξ value changes by $d\xi$ in time dt. If the chemical reaction is the only irreversible process in the system, the increase in entropy should be governed by only $d\xi$ value. Then, according to the second law of thermodynamics, one has

$$dQ = A\,d\xi \geqslant 0.$$

The inequality corresponds to spontaneous occurrence of the reaction, while the equality corresponds to an equilibrium state. This inequality formulated by De Donde[129] introduces the function of state A, which was called the chemical affinity of reaction. For a spontaneous reaction proceeding from the left to the right (for instance, stage 4) at constant pressure and temperature,[58] one has

$$A_{p,T} = -\Delta G_{p,T} = RT\ln\frac{K(T,p)}{(c_2\gamma_2)^{\nu_2}\ldots(c_n\gamma_n)^{\nu_n}} > 0 \qquad (4)$$

where $K(T, p)$ is the equilibrium constant for the process under study, c_i is an arbitrary (*e.g.*, initial) molar concentration of the component i and γ_i is the activity coefficient of the component i. In the case of chemical bath deposition, the initial molar concentrations of components are 10^{-2}–10^{-3} mol litre^{-1}. Since all solutions can be treated nearly ideal when appropriately diluted, one has $\gamma_i \to 1$ and one can use concentrations instead of activity in the chemical affinity calculations. A spontaneous process corresponds to the inequality $A > 0$. Admitting an indubitable hypothesis that the formation of chalcogenide (X) of a divalent metal (M) is described by the equation

$$M^{2+} + X^{2-} \longrightarrow MX\downarrow$$

expression (4) takes the form

$$A = RT\ln\frac{K(T,p)}{[M^{2+}]_0^{-1}[X^{2-}]_0^{-1}} > 0 \qquad (5)$$

where $K(T,p)$ is the equilibrium constant for the formation of solid sulfide MS. Since the solubility product K_{sp} is the equilibrium constant for dissolution of MX precipitate, the equilibrium constant for sulfide formation is $1/K_{sp}$. Using the expressions for the solubility product

$$K_{sp} = [M^{2+}]_{eq}[X^{2-}]_{eq}$$

and the ionic product

$$IP = [M^{2+}]_0[X^{2-}]_0,$$

one gets the equation for the chemical affinity:

$$A = RT\ln\frac{IP}{K_{sp}}$$

In other words, spontaneous formation of metal chalcogenide is possible at supersaturations

$$\Pi = \frac{IP}{K_{sp}} > 1 \quad (6)$$

where $[M^{2+}]_0$, $[X^{2-}]_0$, $[M^{2+}]_{eq}$, $[X^{2-}]_{eq}$ are the initial and equilibrium concentrations of the M^{2+} and X^{2-} ions, respectively.

Thus, in order to discuss the possibility for metal chalcogenide formation to occur, one should determine the initial compositions of the reaction mixture in stages 2 and 3, *i.e.*, the concentrations of the chalcogen and metal ions. This is a nontrivial task because the concentration of chalcogen ions depends on the mechanism of decomposition of the source of chalcogen in stage 3. Kitaev and co-workers [1,3–5] were the first who experimentally showed that decomposition of the main sources of chalcogen (stage 3) is a reversible hydrolysis reaction, determined the equilibrium constants for these reactions and proposed a quantitative thermodynamic substantiation of deposition conditions for many metal chalcogenides. This substantiation appeared to be equally appropriate for the description of systems characterized by the formation of stable complex compounds of metals with the source of chalcogen (with metal–chalcogen coordination) and for systems where no such compounds are formed. Thermodynamic approach is often used for quantitative description of stages 2 and 3.[130]

It is the four stages (see above) taken altogether that are responsible for the mechanism of growth in solution and on substrate, for the chemical composition, structure, microstructure and type of the hybrid form (core–shell, agglomerated nanopowder, isolated particles in colloidal solutions) of solid chalcogenides formed in the reaction.

IV.2. Main sources of sulfide ions

Sulfidizers are compounds which can act as sources of S^{2-} ions in aqueous solutions, *e.g.*, soluble sulfides and hydrosulfides or hydrogen sulfide. However, a necessary condition for preparation of thin-film metal sulfides is low feed rate of S^{2-} ions to the reaction zone. This condition is met using thiocarbonic acid diamide (thiourea) $SC(NH_2)_2$, the best known source of sulfide ions which is widely used for the synthesis of metal sulfide films. The chemical properties and decomposition mechanisms of $SC(NH_2)_2$ are well documented.[130,131] In aqueous alkaline solutions, thiourea undergoes reversible hydrolytic decomposition [1,5,130]

$$SC(NH_2)_2 \rightleftharpoons H_2S + CN_2H_2 \quad (7)$$

In turn, cyanamide CN_2H_2 is hydrolyzed to urea and ammonium carbonate

$$CN_2H_2 + H_2O \rightleftharpoons OC(NH_2)_2$$

$$OC(NH_2)_2 + 2\,H_2O \rightleftharpoons (NH_4)_2CO_3$$

Cyanamide can react with ammonia to give a strong base, guanidine [132]

$$CN_2H_2 + NH_3 \longrightarrow (NH_2)_2C{=}NH$$

Products of these reactions can act as impurities in chemically deposited films. In acid solutions, $SC(NH_2)_2$ decomposes to ammonium ion and thiocyanate ion [133]

$$SC(NH_2)_2 \rightleftharpoons NH_4^+ + SCN^- \quad (8)$$

When reactions are carried out in alkaline media, thiourea derivatives, namely, *N*,*N*′-dimethylthiourea and *N*-allylthiourea,[134] are also used as sources of sulfide ions

$$MeNHC(S)NHMe + H_2O \rightleftharpoons$$

$$\rightleftharpoons MeNHC(O)NHMe + H_2S$$

$$AllNHC(S)NH_2 + H_2O \rightleftharpoons AllNHC(O)NH_2 + H_2S$$

Quite recently, metal sulfides are synthesized in acid media at pH < 4 from sodium thiosulfate $Na_2S_2O_3$. Stability of thiosulfuric acid in aqueous solutions has been a subject of numerous studies reviewed in a monograph.[135] Among various schemes and hypotheses of the mechanism of the process, two primary reactions are usually considered, that is, decomposition of thiosulfuric acid to elemental sulfur and sulfurous acid under the action of strong acids and hydrolysis to hydrogen sulfide and sulfuric acid [136,137]

$$H_2S_2O_3 \rightleftharpoons S + H_2SO_3 \quad (9)$$

$$H_2SO_3 + H_2O \rightleftharpoons H_2S + H_2SO_4 \quad (10)$$

Both reactions do not contradict experimental facts and are therefore considered by many researchers with certainty to be true.

One more worthy source of sulfide ions is thioacetamide $MeC(S)NH_2$, a reagent for deposition of metal sulfides. It is widely used in analytical practice. Unlike the sources of sulfide ions mentioned above, this compound can be hydrolyzed in the whole range of pH values. However, opinions are different as to the mechanism of $MeC(S)NH_2$ hydrolysis.[138] One mechanism is described by the classical reaction [139,140]

$$MeC(S)NH_2 + 2\,H_2O \rightleftharpoons MeC(O)OH + H_2S + NH_3 \quad (11)$$

involving two intermediate stages, *viz.*, the formation of acetamide

$$MeC(S)NH_2 + H_2O \rightleftharpoons MeC(O)NH_2 + H_2S$$

followed by the formation of thioacetic acid

$$MeC(S)NH_2 + H_2O \rightleftharpoons MeC(O)SH + NH_3$$

which is then hydrolyzed to H_2S and MeC(O)OH.

The other mechanism [141] responsible for the appearance of S^{2-} ions in solutions of thioacetamide is described by the reaction

$$MeC(S)NH_2 \rightleftharpoons MeCN + H_2S \quad (12)$$

IV.3. Mechanisms of CdS film formation on substrates

In order not to duplicate information from the available reviews on the thin-film formation mechanisms, we will restrict ourselves to the data reported in the last 15 years and will briefly outline our own views concepts. It is commonly accepted [117, 118, 127, 142–145] that chemical bath deposition of films may follow the ion exchange, cluster (hydroxide, colloidal) and ion-cluster mechanisms.

The ion exchange mechanism is schematically shown in Fig. 12. The formation of CdS film in alkaline solution $SC(NH_2)_2$ is described by the reactions

$$Cd^{2+} + iL^k \rightleftharpoons (CdL_i)^{2+ik} \quad (13)$$

$$SC(NH_2)_2 + 2HO^- \rightleftharpoons S^{2-} + CN_2H_2 + 2H_2O \quad (14)$$

$$Cd^{2+} + S^{2-} \longrightarrow CdS \quad (15)$$

Clearly, reaction (15) requires that IP > K_{sp} for CdS [see Eqn (6)]. Once this condition is met, CdS particles are formed directly on the substrate (Fig. 12) and adhesion of solid CdS to the substrate is, generally, due to van der Waals forces. In some cases, chemical and electrostatic interactions between ions and substrate are possible; for instance, using a gold plate as substrate, one can expect the formation of Au–S bonds on the surface.

The cluster (colloid) mechanism assumes nucleation of a solid phase, formation of solid-phase clusters immediately in the homogeneous solution and subsequent growth, coagulation and adsorption of clusters on the substrate surface.[80, 130] The chemical composition of the clusters is governed by the synthesis conditions. Namely, chemical bath deposition using $MeC(S)NH_2$ and thiosulfate ion ($S_2O_3^{2-}$) as sources of sulfide ions at pH < 5 leads to formation of sulfide clusters and metal hydroxide in alkaline solutions. The formation of metal hydroxide is hard to avoid under experimental conditions despite the presence of complex-forming agents;[6, 146] therefore, this mechanism is sometimes called hydroxide mechanism (Fig. 13).[142] In this case, complexation (13) and hydrolysis of $SC(NH_2)_2$ (14) are accompanied by the reaction

$$Cd^{2+} + 2OH^- \longrightarrow Cd(OH)_2 \quad (16)$$

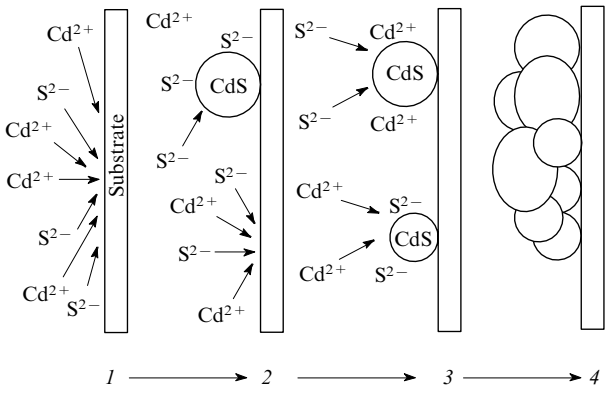


Figure 12. Ionic mechanism of CdS film formation on substrate.[142] Diffusion of Cd^{2+} and S^{2-} ions towards substrate (*1*); reaction between Cd^{2+} and S^{2-} ions with the formation of a nucleus of solid CdS (*2*); growth of CdS nucleus by adsorption of Cd^{2+} and S^{2-} ions (*3*); and coagulation of CdS particles due to van der Waals forces (*4*).

and the formation of metal sulfide is not described by Eqn (15). Here, one gets:

$$Cd(OH)_2 + S^{2-} \longrightarrow CdS + 2OH^- \quad (17)$$

Transformation of metal hydroxide to metal sulfide is only possible if K_{sp}(metal hydroxide) > K_{sp}(metal sulfide) because the solubility product of CdS (pK_{sp} = 26.10) much exceeds that of freshly deposited $Cd(OH)_2$ (pK_{sp} = 13.66). Kitaev *et al.*[1, 3, 4] established that the formation of CdS films using $SC(NH_2)_2$ as source of sulfide ions proceeds *via* the metal hydroxide route. On the one hand, the hydroxide layer has undesired effect on the functionality of semiconductor devices, in particular, CIGSSe solar cells where CdS thin films are used as the 'window layer'.[6] On the other hand, with no hydroxide layer the CdS film loses its adhesive properties.

The ionic and colloid mechanisms assume homogeneous nucleation. However, studies on the kinetics of deposition under spontaneous solid phase formation showed that

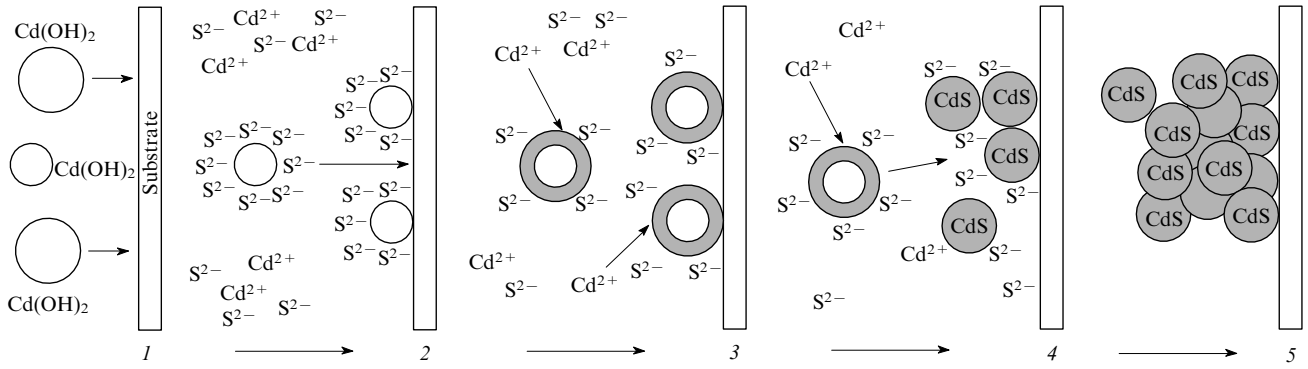


Figure 13. Cluster (hydroxide, colloidal) mechanism of CdS film formation on substrate.[142]
Diffusion of $Cd(OH)_2$ colloidal particles induced by Brownian motion towards the substrate; adsorption of particles (*2*); and interaction of particles with S^{2-} ions (*3*). The S^{2-} ions are formed either upon homogeneous hydrolysis of the source of sulfide ions or in heterogeneous reaction where $Cd(OH)_2$ particles can act as catalyst of hydrolysis of the source of sulfide ions. As a result, exchange of hydroxide ions for sulfide ions proceeds on the substrate surface and in bulk solution (*4*) and CdS film is formed (*5*).

formation of metal sulfides is a heterogeneous autocatalytic process.[147–149] This is an indication of more complicated, mixed mechanisms of film formation. It should be noted that the fundamental difference between the mixed mechanism and the simple cluster (hydroxide, colloidal) mechanism consists in that metal sulfide is formed not only due to consumption of free S^{2-} ions [see reaction (14)]. The mixed mechanism assumes the possibility for the source of sulfide ions, in particular, $SC(NH_2)_2$, to adsorb on the surface of solid $Cd(OH)_2$ particles {or on $[(CdOH)_2(NH_3)_2]$ particles},[144] thus forming metastable surface complex compounds which then decompose with the formation of CdS.[150] Based on the available experimental data, the 'hydroxide mechanism' of CdS film deposition proposed earlier [1, 3, 4] can be written as follows:[150]

$$\begin{aligned} &Cd(NH_3)_4^{2+} + 2\,OH^- + site \rightleftharpoons Cd(OH)_{2,ads} + 4\,NH_3 \\ &Cd(OH)_{2,ads} + SC(NH_2)_2 \longrightarrow [Cd(OH)_2SC(NH_2)_2]_{ads} \\ &[Cd(OH)_2SC(NH_2)_2]_{ads} \longrightarrow \\ &\quad \longrightarrow CdS + H_2CN_2 + 2\,H_2O + site \end{aligned} \qquad (18)$$

or in the following way:[78]

$$\begin{aligned} &Cd^{2+} + site + 2\,OH^- \longrightarrow Cd(OH)_{2,ads} \\ &Cd(OH)_{2,ads} + SC(NH_2)_2 \longrightarrow C^* \longrightarrow CdS + site \end{aligned} \qquad (19)$$

where ads are compounds adsorbed on the substrate; C* is the intermediate; site is the surface of a silicon or glass substrate onto which the CdS film is deposited.

It should be noted that Eqn (19) describing the mixed mechanism of film formation includes two undefined[143] 'parameters', *viz.*, $Cd(OH)_{2,ads}$ and C*. Experiments[151] showed that gradual adsorption of atomic layers of the $Cd(OH)_2$ film on the surface of the oxygen-containing substrate results in the formation of a common layer of composition $Cd(OH)_2/SiO_2$. Taking into account the fact[152] that direct interaction of SiO_2 with the cadmium salt in aqueous alkaline solutions mainly results in cadmium silicate $Cd(SiO_2)_n$ with a SiO_2 : Cd mole ratio of about 1 : 1, the $Cd(OH)_{2,ads}$ phase in Eqn (19) corresponds to $Cd(OH)_2/Cd(SiO_2)_n/SiO_2$ provided that deposition occurs onto a silicon or glass substrate. Subsequent sulfidizing of the surface of this cadmium-containing layer on the substrate produces a precursor layer (denoted by C*) representing a $CdS/Cd(OH)_2/Cd(SiO_2)_n/SiO_2$ intermediate layer (Fig. 14). Initial adhesion of the bottom atomic layers of $Cd(OH)_2$ to the oxygen-containing substrate film and partial sulfidizing of the top layers of $Cd(OH)_2$ ensure growth of the CdS film and strong adhesion to the substrate. Further sulfidizing of this layer and a complete conversion of the hydroxide to sulfide causes the adhesive force to vanish and the CdS film can be removed from the substrate with ease.

We believe that chemical deposition of CdS thin films from aqueous alkaline solutions onto silicon or glass substrates necessarily involves the formation of compound $Cd(OH)_2$ as the intermediate layer provided that the substrate was not pretreated.[118, 153] Then, it is the mixed mechanism of film formation described by Eqn (19) that

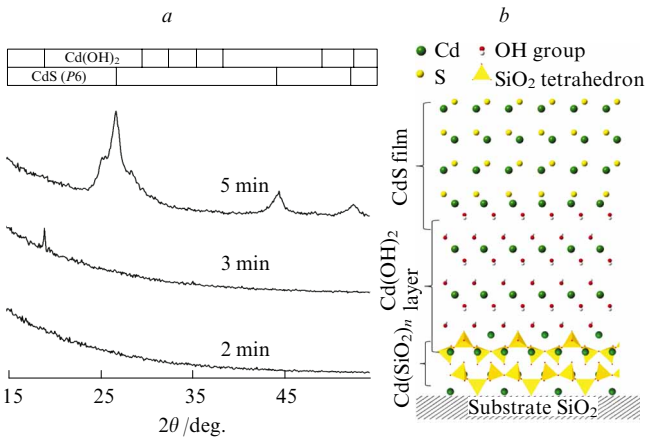


Figure 14. Growth mechanism of CdS film on the $Cd(OH)_2/Cd(SiO_2)_n/SiO_2$ precursor layer deposited on glass substrate. (*a*) Grazing incidence X-ray diffraction patterns from a series of thin films prepared at different temperatures;[151, 153] all X-ray diffraction patterns were measured from the bottom side of the substrate; top: positions of the peaks from the average lattice of the rcp structure of nano-CdS (space group *P*6) and from the hexagonal structure of cadmium hydroxide (space group $P\bar{3}m1$); (*b*) model of a film on substrate.[154]

seems to be the most plausible. In revised form, it can be written as follows:

$$\begin{aligned} &Cd^{2+} + 2\,OH^- + site \longrightarrow Cd(OH)_2 \xrightarrow{SiO_2,\ adhesion} \\ &\quad \longrightarrow Cd(OH)_2/Cd(SiO_2)_n/SiO_2 \\ &S^{2-} + Cd(OH)_2/Cd(SiO_2)_n/SiO_2 \longrightarrow \\ &\quad \longrightarrow CdS/Cd(OH)_2/Cd(SiO_2)_n/SiO_2 \xrightarrow{OH^-,\ sulfide\ formation} \\ &\quad \longrightarrow CdS-SiO_2/Si \\ &Cd^{2+} + S^{2-} + Cd(OH)_2/Cd(SiO_2)_n/SiO_2 \longrightarrow \\ &\quad \longrightarrow CdS + Cd(SiO_2)_n/SiO_2 + site \end{aligned} \qquad (20)$$

IV.4. Mechanisms of formation of CdS nanoparticles

Chemical bath deposition belongs to 'bottom – up' methods of fabrication of nanostructured materials.[155] Here, nanoparticles are formed from atoms and molecules, *i.e.*, by growth of seeds to nanoparticles. Cadmium sulfide nanoparticles, as well as other metal sulfide nanoparticles, can be synthesized by aqueous solution deposition using reactions of soluble metal compounds with sulfidizing agents (see Section VI.2). Various groups of sulfidizers only differ in that the precipitating agent (S^{2-} ion) is either added to the solution containing ions being deposited ($[CdL_i]^{2+ik}$ or Cd^{2+}) or is gradually formed in the course of hydrolysis proceeding in the bulk solution. It is hydrolyzable sources of sulfide ions that are used for film synthesis. However, solid particles that are formed in the reaction not only form the film on the substrate surface or on reactor walls, but also coagulate with the formation of powder-like precipitate in bulk solution. In this case, typical kinetic curves have an S-shape characteristic of autocatalytic processes in which the role of catalyst is played by the surface of the solid phase

(CdS).[147] The rate of sulfide formation in the system is proportional to the surface area of the solid phase nucleating in bulk reaction mixture and to the concentrations of the main reactants, that is, the complex salt $[CdL_i]^{2+ik}$ and $SC(NH_2)_2$. Therefore, the reaction rate can be described by the model second-order equation written using the concentrations of metal and $SC(NH_2)_2$ in the solution [147, 148]

$$\omega = \frac{d(c_{M,0} - c_M)}{d\tau} = K_{ex}(c_{M,0} - c_M)^{2/3} c_M c_{Thio} \quad (21)$$

where ω is the rate of metal sulfide formation in the solution, K_{ex} is the experimental rate constant for the reaction, $c_{M,0}$ and c_M (mol litre^{-1}) are the concentrations of metal ions in the solution at $\tau = 0$ and at an arbitrary instant ($\tau > 0$), respectively; $c_{Thio,0}$ and c_{Thio} (mol litre^{-1}) are the concentrations of $SC(NH_2)_2$ at $\tau = 0$ and at $\tau > 0$, respectively; $(c_{M,0} - c_M) = (c_{Thio,0} - c_{Thio}) = x$ is the amount of metal sulfide formed during the time interval τ since the beginning of the reaction, in mol litre^{-1}; and $(c_{M,0} - c_M)^{2/3} = x^{2/3}$ is the quantity proportional to the surface area of the metal sulfide particles seeded in the homogeneous solution.

Assuming a spherical shape of the particles of the nucleating solid phase, their number remains constant, while the mass and surface area of each particle increase due to precipitation of metal sulfide formed in the reaction. The kinetic equation for the synthesis of CdS in alkaline solutions of $SC(NH_2)_2$ has the form [147]

$$\frac{dx}{d\tau} = 1.27 \times 10^{17} \exp\left(-\frac{78000}{8.3147T}\right) x^{2/3} c_{NH_3}^{-3} c_{OH^-} (c_{Cd,0} - x) \times \quad (22)$$

$$\times (c_{Thio,0} - x)$$

where c_{NH_3}, c_{OH^-} are respectively the concentrations of NH_3 and OH^- ions at $\tau = 0$, mol litre^{-1}.

If only one (sulfide) crystalline phase is formed, CdS in solutions of $SC(NH_2)_2$ forms much more slowly than in the solution of Na_2S containing the 'available' ions (S^{2-} and HS^-). For instance, the formation of CdS using Na_2S at room temperature is observed a few seconds after the beginning of the reaction (*cf.* a few minutes for solutions of $SC(NH_2)_2$ and mixing of reactants). The use of $SC(NH_2)_2$ leads to low initial supersaturation, small amount of crystal nuclei, while subsequent hydrolysis of $SC(NH_2)_2$ causes growth of the available particles rather than nucleation of CdS.

The use of $SC(NH_2)_2$ leads to low initial supersaturation, small amount of crystal nuclei, while subsequent hydrolysis of $SC(NH_2)_2$ causes growth of the available particles rather than nucleation of CdS. This suggests the existence of a limiting stage of hydrolysis of $SC(NH_2)_2$. The growth rate of CdS particles is described by the second-order equation with respect to the main components involved in the reaction [see Eqn (21)]. Also, it is proportional to the initial concentrations of reactants, *i.e.*, to the chemical affinity of reaction, A. Thus, in solutions of $SC(NH_2)_2$, nuclei of the solid phase grow much faster than nucleation occurs and the particle size increases with increasing A. This leads to formation of larger particles compared to those produced by deposition using Na_2S.[155] If initially the starting solution contains S^{2-} ions produced by dissociation of Na_2S in the preparation step, the formation of sulfide nanoparticles obeys the classical theory of precipitation and the Weymarn–Haber precipitation rule, according to which the nanoparticle size decreases with increasing A.[156]

The kinetic equation (22) and insights into the influence of the affinity A on the nanoparticle size are valid if only one crystalline phase, *e.g.*, CdS is formed in the solution. However, the first solid phase formed in alkaline solutions is often $Cd(OH)_2$ (Fig. 15). Since it is formed in bulk solution, it is clear that not only the film, but also powder-like precipitate will contain cadmium hydroxide. The $Cd(OH)_2$ phase can influence the morphology of CdS single crystals and polycrystalline CdS particles,[157] which in turn may govern the electronic, optical and magnetic properties of materials [158] and thus the laws of chemical, physical and biological processes.

In Fig. 15, the concentration region between the surfaces *I* and *II* corresponds to formation of a single phase, namely, CdS. Chemical bath deposition using $SC(NH_2)_2$ produced only wurtzite CdS powders in this concentration region; no CdS films visible to a naked eye were formed. The average size of the CdS particles formed in this concentration region was determined using X-ray diffraction data and averaged over all *hkl* directions. It appeared to be larger than 9 nm. This is to some extent erroneous estimate of the particle size. Indeed, as the particle size decreases to a few nanometres, the proportion of surface atoms abruptly increases, which causes the shape of particles to change.[160, 161] Cadmium sulfide nanoparticles have a complex shape, *viz.*, they are extended along the [001] axis, which leads to a large proportion of the (100) and (110) lateral faces.[94] The concentration region of H^+ ions (c_{H^+}) and complex-forming agent (ammonia) ions (c_{NH3}) below surface *I* corresponds to co-deposition of CdS and $Cd(OH)_2$ with the formation of CdS powders and films with the rcp structure and particles smaller than < 9 nm in size (see Fig. 15). The shape of CdS particles with the rcp structure was simulated by random superposition of hexagonally packed atomic layers, which led to hexagonal prismatic shape of the model particles.[94]

Thus, aqueous solution deposition using $SC(NH_2)_2$ under conditions where no $Cd(OH)_2$ is formed produces wurtzite CdS powders with particles larger than 9 nm in size. If the formation of $Cd(OH)_2$ is thermodynamically allowed, both CdS powders and thin films can form. Here, CdS particles have the rcp structure, being smaller than 9 nm in size. Cadmium sulfide particles synthesized using Na_2S as the source of sulfide ions are also smaller than 9 nm and have the rcp structure. It should be noted that CdS particles with the rcp structure are formed due to the decrease in the average particle size [94] rather than the presence of $Cd(OH)_2$.

Cadmium sulfide particles produced by chemical bath deposition can form polycrystals of regular shape (see, *e.g.*, hexagonal prisms with an edge length of 2 μm shown in Fig. 16 *a*,*c*).[53] The presence of so large agglomerates was explained [53] by self-organization of 6-nm CdS nanoparticles; however, we believe that it is an erroneous point of view. The reasons are as follows.

A $Cd(OH)_2$ particle deposited under the same conditions as CdS particles,[53] except introduction of sulfidizer into the solution, had a hexagonal prismatic shape (see Fig. 16 *b*). We believe this shape is inherited by agglomerates of CdS nanoparticles formed in the course of sulfidizing of

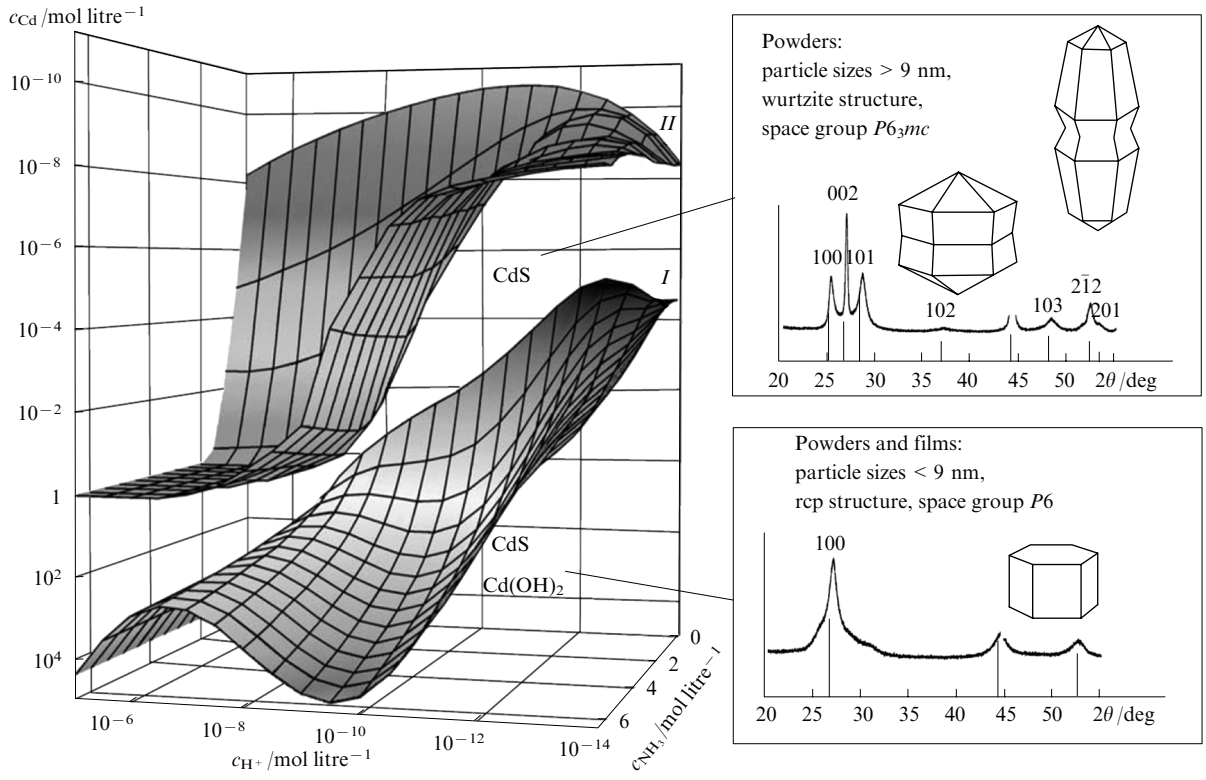


Figure 15. Equilibrium concentration of Cd^{2+} ions ion aqueous solution plotted *vs.* concentrations of H^+ ions and complex-forming agent (ammonia).[159]
Insets: shape of CdS particles determined from X-ray diffraction data.[94] CdS particles were prepared by chemical bath deposition using $SC(NH_2)_2$.

$Cd(OH)_2$ in aqueous solution using $SC(NH_2)_2$. The formation of CdS particles of regular shape in the presence of $Cd(OH)_2$ (Fig. 16 *d*) was also observed earlier (see Refs 141, 162, 163).

The mechanism of formation of regularly shaped monodisperse polycrystalline CdS particles in aqueous $Cd(OH)_2$ sol using thioacetamide as source of sulfide ions and ammonia and/or ethylenediaminetetraacetic acid (EDTA) as complex-forming agents was for the first time studied by Sugimoto *et al.*[141] It was shown [141, 162, 163] that the addition of $MeC(S)NH_2$ to the $Cd(OH)_2$ sol is followed by instantaneous formation of CdS nuclei that grow without coagulation, *i.e.*, the number of CdS nuclei remains the same and can only be changed by adding a new portion of $MeC(S)NH_2$. Cadmium sulfide nuclei are formed in the reaction between S^{2-} and Cd^{2+} ions produced upon hydrolysis of $MeC(S)NH_2$ and dissolution of $Cd(OH)_2$, respectively. Cadmium hydroxide is dissolved through complexation. These results clearly demonstrate that growth of CdS nuclei in the presence of $Cd(OH)_2$ involves three elementary steps, *viz.*, dissociation of complex cadmium ions; diffusion of free Cd^{2+} cations and a surface reaction of S^{2-} with Cd^{2+} rather than proceeds by the Ostvald ripening mechanism.

Nucleation and growth of nuclei can be described by the overall reaction [141]

$$MeC(S)NH_2 + Cd(OH)_2 \longrightarrow CdS + MeCN + 2\,H_2O \quad (23)$$

Studies on the kinetics of $Cd(OH)_2$ transformation to CdS in aqueous thiourea solutions using NH_3 as complex-forming agent showed that the relative content of $Cd(OH)_2$ in the precipitate decreases while that of CdS increases with deposition time.[159, 164] From the data shown in Fig. 17 it follows that almost no cadmium sulfide is formed within 1 min since the start of deposition because in the presence of $Cd(OH)_2$, the process a limiting stage is dissociation of complex cadmium ions rather than hydrolysis of the source of sulfide ions.[163] Then, CdS is synthesized in the reaction between free cadmium ions and sulfide ions. The formation of insoluble sulfide shell on $Cd(OH)_2$ particles precludes further dissolution of cadmium hydroxide, the concentration of cadmium ions decreases and the sulfidizing process slows down. The CdS : $Cd(OH)_2$ ratio in the $Cd(OH)_2$/CdS heterostructure depends on the deposition time, all things considered, and can be fixed at any time by terminating the reaction.

These data provide convincing proofs that the presence of regularly shaped polycrystals in CdS powder (see Fig. 16 *a*,*c*) is due to the transformation of single-crystalline $Cd(OH)_2$ particles to CdS in aqueous solutions of sulfidizers.

IV.5. Aqueous colloidal solutions of CdS: mechanisms of formation

Methods for synthesis of isolated nanocrystals based on Group II – VI element chalcogenides (CdSe, CdTe, CdS and ZnSe) in liquid media have long been known. In particular, Bawendi and co-workers.[165] for the first time reported a

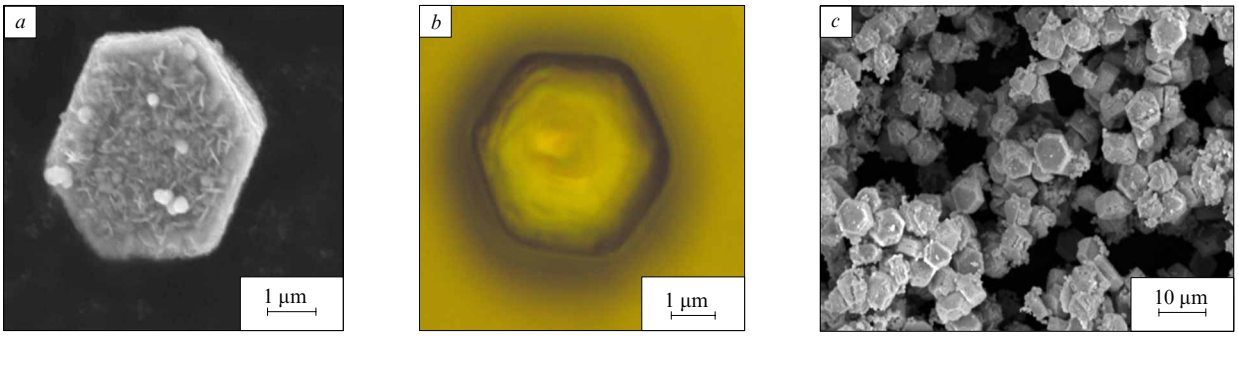


Figure 16. CdS particles (*a*, *c*) and $Cd(OH)_2$ (*b*, *d*).
(*a*) Scanning electron microscopy image of an agglomerate of CdS nanoparticles which inherits the prismatic shape from $Cd(OH)_2$ single crystal. The agglomerate has a shape of a hexagonal prism with an edge length of 2 μm and consists of coagulates 200–300 nm in size. According to transmission electron microscopy and X-ray diffraction data, coagulates comprise 6-nm crystalline CdS nanoparticles;[158]
(*b*) hexagonal prismatic single crystal of cadmium hydroxide $Cd(OH)_2$; all edges have almost the same length of 3 μm. $Cd(OH)_2$ powder was prepared from aqueous solutions of complex salt $Cd(NH_3)_n^{2+}$ and NaOH at pH 13 (original optical microscope image obtained by the authors of this review; first publication);
(*c*) CdS agglomerates;[158]
(*d*) photomicrograph of regularly shaped CdS polycrystals prepared under normal conditions by sulfidizing of $Cd(OH)_2$ with thioacetamide as source of sulfide ions and NH_3 and EDTA as complex-forming agents.[163]

method for synthesis of high-quality colloidal chalcogenide nanoparticles in organic solvents in the presence of trioctylphosphine oxide (TOPO). This is the so-called high-temperature organometallic synthesis. Owing to small size of nanocrystals the synthesis is accompanied by intense agglomeration and subsequent coagulation and coalescence (multiple increase in size) of nanoparticles. The problem is solved by coating nanoparticles with a TOPO layer but nanocrystals thus become soluble solely in organic solvents (chloroform, toluene, heptane, *etc*.). They can be used in biological media only after surface modification by attachment of hydrophilic groups. This underlies the development of methods for stabilization and solubilization of such particles.

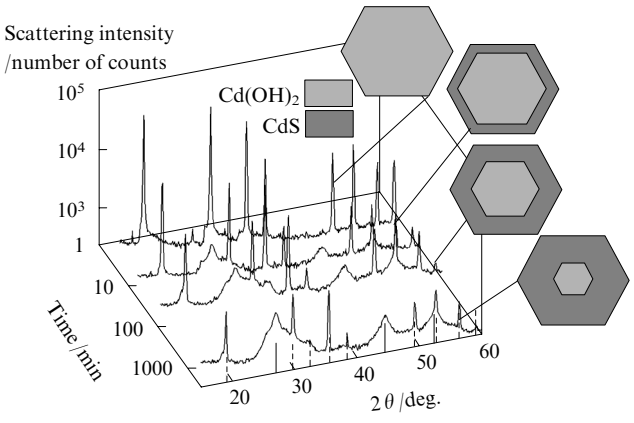


Figure 17. Growth of core–shell heterostructure $Cd(OH)_2$@CdS as function of deposition time according to results of analysis of the X-ray diffraction patterns of precipitates collected after 6, 20, 120 and 2880 min of deposition.[164]
Diffraction reflections from the rcp phase of CdS and hexagonal cadmium hydroxide $Cd(OH)_2$ are denoted by solid and dashed lines, respectively. The scattering intensities and time are shown in the logarithmic scale. Cu$K_{\alpha 1,2}$ radiation.

Main methods for solubilization of nanocrystals make use of the following three approaches:[12]

— utilization of bifunctional compounds capable of replacing TOPO molecules and containing hydrophilic groups that are exposed to solution after attachment to nanocrystals and thus provide solubility in water;

— formation of a polymer shell surrounding the nanocrystal by penetration of hydrophobic fragments of solubilizing agents into the TOPO layer without removal of the TOPO molecules from the surface of nanocrystals; and

— encapsulation of semiconductor nanocrystals into polymer microparticles (microspheres or microcapsules).

Replacement of TOPO by bifunctional ligands is based on the adsorption of ligands containing thiol or phosphine groups (mercapto acids, cysteine, *etc*.) or SH groups (chemically modified ethylene glycol, DNA, proteins or peptides) to form bonds with the surface metal or sulfur atoms.[12, 21, 22, 166] Solutions of these ligands are added to TOPO-coated nanocrystals in chloroform. The formation of bonds between sulfur atoms and the surface metal or sulfur ions leads to replacement of TOPO molecules by the solubilizing ligands. As a result, nanocrystals precipitate from the organic solvent. The precipitate is water soluble and the nanocrystal shell includes reactive groups for conjugation with biomolecules (antibodies, DNA, RNA, proteins, *etc*.) (Fig. 18). A method is available that combines polyvalent bonding with subsequent formation of a polymer shell around the nanocrystal.[167] The surface of nanocrystals is coated with a silica/siloxane layer and then siloxane groups are polymerized to be covalently bound to methoxy compounds (*e.g*., aminopropyltrimethoxysilane). Polysiloxane-coated nanocrystals are very stable.

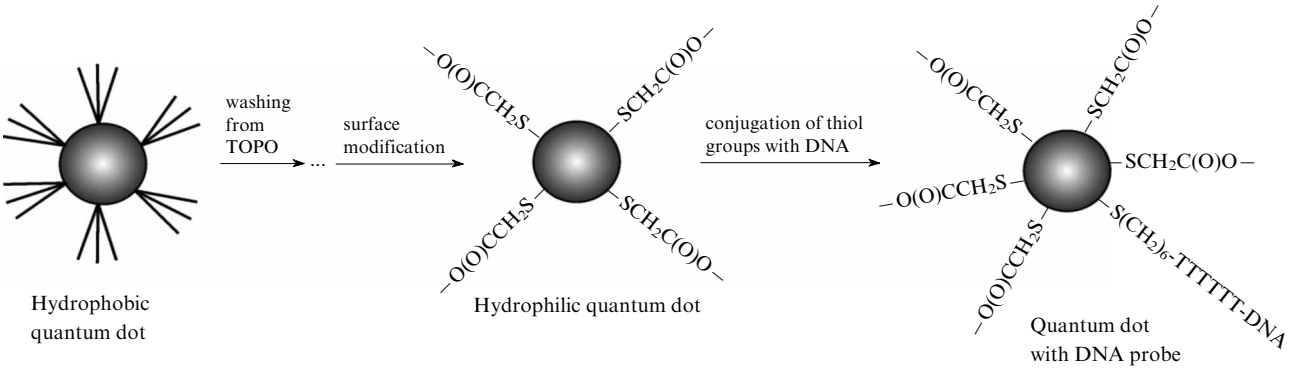


Figure 18. Modification of quantum dots for conjugation with DNA for analysis by *in situ* fluorescence hybridization.[167, 168] The quantum dot surface is washed to remove TOPO and then is covered with sulfide groups to bind biomolecules.

The second approach (formation of 'insulating' polymer layer around nanocrystals) uses hydrophobic character of the TOPO molecules present on the surface of nanoparticles in order to bind hydrophobic fragments of bifunctional solubilizing polymers, *e.g.*, multiblock copolymers, polyethylene glycol (PEG), *etc.* (Fig. 19). Hydrophilic fragments of these molecules exposed to the surrounding aqueous solution form a polar shell[169] containing reactive groups for covalent attachment of biomolecules (antibodies, biotin, streptavidin, peptides, DNA).

Encapsulation of nanocrystals into submicrometre and micrometre polymer particles (third approach) not only makes it possible to utilize conventional methods of organic synthesis for covalent attachment to functional groups of biomolecules, but also enables isolation of nanocrystals from the environment and their stabilization in aqueous solutions. By filling each microsphere with a specified amount of nanocrystals with particular photoluminescence colour one can practically implement multiple spectral encoding. To embed semiconductor nanocrystals into polymer matrices, it was proposed to use molecular encapsulation (formation of micelles with encapsulated nanocrystals).[12, 22] The technique is based on the growth of nanocrystals immediately in the polymer matrix. Cadmium sulfide nanoparticles can be stabilized by chelating groups[170] or by amino groups of block copolymers,[171] as well as by dendrimers based on amine macromolecules with the amino groups acting as stabilizers (Fig. 20).

The major drawbacks of the solubilization of nanocrystals include complexity and long duration of the process, high loss of materials and a low yield of solubilized nanocrystals. Semiconductor nanoparticles can be synthesized by CBD involving preparation of aqueous colloidal solutions of CdS with high aggregative and sedimentation stability using the one-pot approach. Unlike organometallic synthesis, chemical bath deposition is carried out at room temperature with aqueous $CdCl_2$ solution as the source of cadmium instead of $Cd(Me)_2$, which is toxic, pyrophoric and unstable at room temperature. Coagulation of CdS nanoparticles is prevented by introducing stabilizing agents (ligands for Cd^{2+} ions) including phosphates, thiols, amino acid derivatives and hydrophilic polymers into the solution and using H_2S, thiourea and Na_2S as the sources of sulfide ions.[98, 173–180] Among stabilizers, a particular position is occupied by two biomolecules, cysteine and glutathione (GSH), which simultaneously impart hydrophilic and biocompatible properties to CdS nanoparticles.[98, 174, 178] Dur-

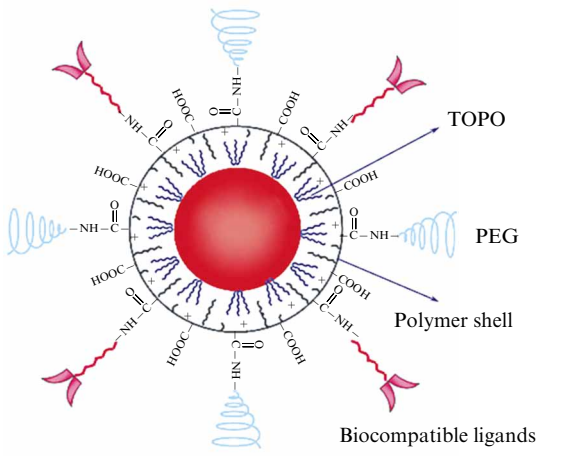


Figure 19. Formation of hydrophilic polymer layer around the quantum dot.[169]
Quantum dot structure: the core is surrounded by TOPO layer with attached amphiphilic polymer layers composed of PEG and a block copolymer with biocompatible functional groups.

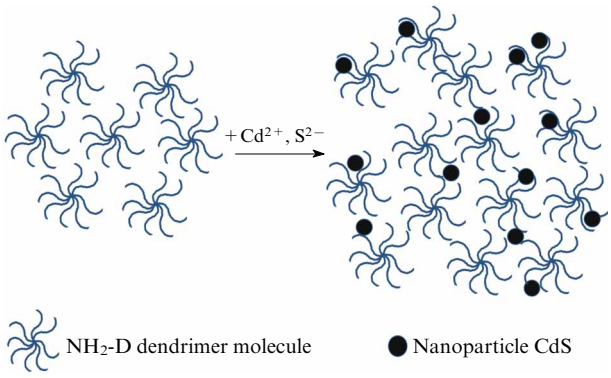


Figure 20. Stabilization of CdS nanoparticles in aqueous solution by molecules of a star-like dendrimer based on polyamidoamine (generation: $g = 4.0$, 64 terminal amino groups) NH_2-D.[172]

ing the synthesis, GSH first of all plays the role of a polydentate ligand [174, 178] with respect to Cd^{2+} ions. Recently, it was proposed to use GSH as sulfidizing agent.[178] Chemical bath deposition of water-soluble CdS nanoparticles in alkaline GSH solutions at different pH values is schematically shown in Fig. 21.

The first step (see Fig. 21 *a*) involves the formation of a Cd^{II}–GSH coordination polymer using coordination interaction between Cd^{2+} and GSH ions. Here, Cd^{2+} binds to thiol groups and can form a peptide bond between cycteine amino group and glutamine carboxyl group. In the next step, the addition of NaOH to the Cd^{II}–GSH colloidal solution is followed by cleavage of the peptide bond, isolation of sulfur and formation of the CdS–GSH quantum dot.

Different types of coordination bond can be formed in the first step depending on the pH value (see Fig. 21 *b*). As the pH value increases, the size of spherical particles of the Cd^{II}–GSH polymer decreases while that of CdS nanocrystals increases.[178]

The reasons for water solubility of hydrophobic quantum dots prepared by chemical bath deposition are as follows. Stabilizing agents on the surface of quantum dots orient the surrounding polar water molecules, thus creating an additional hydrophilic solvation (hydration) shell. Thus one deals with the adsorption-solvation stability factor of the colloidal solution.

However, the formation of strong complexes may also cause more intense decomposition (dissolution) of the dispersed phase formed by nanoparticles. For instance, EDTA as chelating agent [179, 180] can retard the formation and growth of CdS nanoparticles in the synthesis of CdS colloidal solutions. EDTA present in the solution is responsible for the occurrence of two competing reactions, namely, complexation between Cd^{2+} ions and EDTA and dissolution of CdS nanoparticles; the colloidal solution is characterized by a dynamic equilibrium between dissolution and formation of the dispersed CdS phase.

It is convenient to describe colloidal solutions using the term 'micelle' to show that the case in point is the structure of hydrophobic particles of insoluble solid CdS present in the aqueous solution and to distinguish them from powder particles ('dry' particles) formed after removal of the dispersed medium. Taking into account the experimentally measured negative value of the ζ-potential, it was proposed [180] to denote the micelle of CdS colloidal solution prepared in the presence of EDTA as follows:

$$\{[CdS]_m \cdot 2n\,Cd(EDTA)^{2-} \cdot (2n - x)Na^+_{aq} \cdot (2n - x)\,H^+_{aq}\}^{2x-} \cdot$$
$$\cdot x\,Na^+_{aq} \cdot x\,H^+_{aq}$$

where $m \geqslant 1$.

The $Cd(EDTA)^{2-}$ chelates adsorbing on the surface of CdS nanoparticles and imparting a negative charge to the

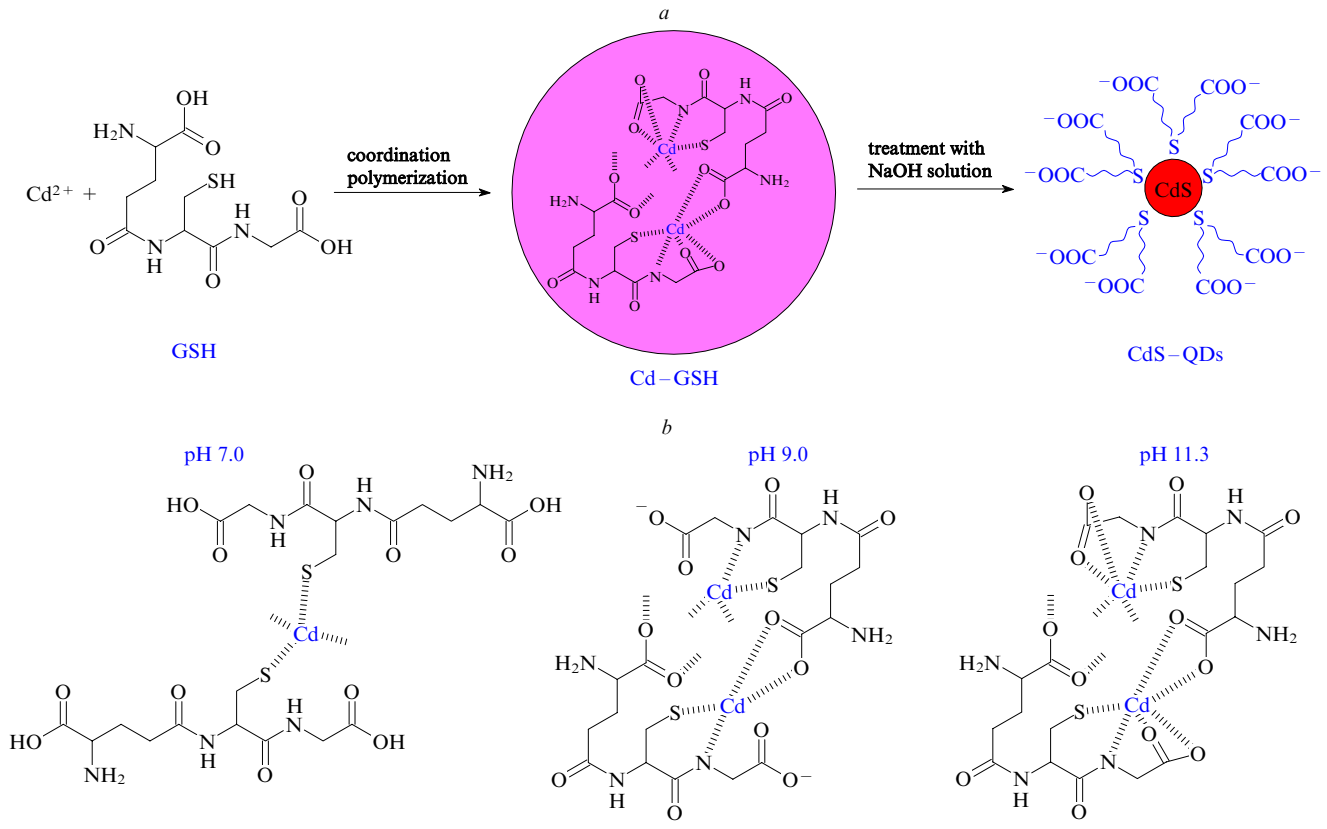


Figure 21. Formation of water-soluble CdS–GSH nanoparticles by alkaline hydrolysis of Cd^{II}–GSH coordination polymer at pH 11.3 (*a*) and types of coordination bond between Cd^{2+} ions and GSH molecules in Cd^{II}–GSH particles at different initial pH values of the GSH solutions (*b*).[178]

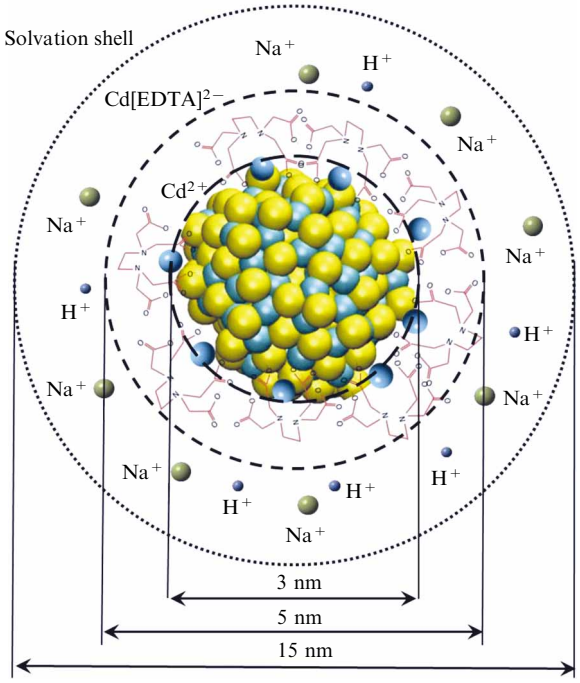


Figure 22. Model structure of CdS micelle based on theoretical [62] and experimental [180] data.

micelle cores preclude the approach of S^{2-} anions to the micelle cores, thus precluding aggregation of nanoparticles and growth of the CdS crystal. Cadmium sulfide nanoparticles with anions adsorbed on them become aggregatively stable. From the micelle formula given above it follows that the species comprises a CdS aggregate consisting of CdS nanoparticles, a layer of potential-determining ions (organic shell), as well as the adsorption and diffuse layers of hydrated counterions (solvation shell) (Fig. 22).

Summing up, chemical bath deposition makes it possible to prepare water-soluble CdS particles in colloidal solutions. The diffraction patterns of the dispersed CdS phase of these solutions [104,178,180] exhibit clearly seen halo indicating a large proportion of 3-nm particles with amorphous structure similar to that reported by Junkermeier *et al.*[62]

V. Conclusion

Interest in nanostructured cadmium sulfide aroused in the early 1990s is due to potential solar-cell applications of the optical properties of thin films. At that time, the best methods for preparation of thick photo-active CdS films were based on the method of CBD developed by researchers from the Ural Region (USSR) in the 1970s. To the early 2000s, the focus in possible applications of quantum dots shifted to the design of biosensors and biomarkers and the luminescent properties of quantum dots appeared to be of crucial importance. To optimize the optical properties, various procedures for the synthesis of CdS quantum dots were elaborated. Preparation of nanostructured forms of CdS went far beyond the field of chemical bath deposition. The late 2000s were marked by pioneering efforts in developing novel applications of quantum dots, namely, photocatalysis and sensitization of solar cells. Intensification of research in these fields was accompanied by renewal of interest in aqueous solution deposition of CdS as promising method for synthesis of quantum dots for these applications.

Among the bottom–up technologies used for preparation of nanostructured materials from atoms and molecules, the CBD method is simple, cheap and allows one to synthesize various bulk and nanostructured hybrid forms of semiconductor compounds including CdS. These can be continuous and island-type films on surfaces of any size and configuration, core–shell structures, agglomerated polycrystals of regular shape, as well as isolated particles in colloidal solutions. Depending on the type of the source of sulfide ions, the chemical affinity and the possibility of competing formation of other solid phases, one can synthesize CdS particles of different size and different structure (Fig. 23).

Fundamentally, different groups of the sources of sulfide ions only differ in that the precipitating agent (S^{2-} ion) is either added to the solution containing complex cadmium ions being deposited or it is slowly and gradually formed in bulk solution due to hydrolysis of sulfidizers. It is hydrolyzable sources of sulfide ions that are used for the synthesis of CdS films.

An important role in the chemical bath deposition is played by cadmium hydroxide $Cd(OH)_2$. If the formation of $Cd(OH)_2$ is thermodynamically impossible, wurtzite CdS powders with particles > 9 nm in size are formed. The critical minimum size, 9 nm, is due to high degree of distortion of sp^3 orbitals, which is characteristic of just wurtzite structure.

If the formation of $Cd(OH)_2$ is thermodynamically allowed, both CdS powders and thin films can form. Here, CdS particles are from 3 to 9 nm in size and have the rcp structure characterized by random sequence of packing layers. The short-range order and tetrahedral environment of cadmium and sulfur atoms play the decisive role for the particle structure and the atomic arrangement can be interpreted as the 'average' long-range order. In the case of film formation, cadmium hydroxide forms a necessary intermediate layer between the CdS film and substrate. The presence of $Cd(OH)_2$ in solution during the deposition of crystalline phase and gradual sulfidizing of this phase leads to formation of nanostructured CdS microparticles of a regular shape. The formation of CdS occurs on the surface of $Cd(OH)_2$ crystals in the presence of complex-forming agents.

Particles $\sim 2-3$ nm in size can form stable colloidal solutions. They have almost amorphous structure owing to a large proportion of surface atoms. The scheme in Fig. 23 illustrates the possibility of controlling the size of CdS particles with specified structure in the course of CBD process. The methods described above can be used in the design of experiments on the synthesis of CdS and other heavy-metal sulfides in aqueous solutions.

The synthesis of CdS nanoparticles with specified size and structure offers prospects for controlling their properties. The surface and size effects influence the properties of CdS nanoparticles in different manner irrespective of the method of synthesis. In particular, the optical absorption edge and, correspondingly, the band gap in CdS nanoparticles are determined solely by the size factor. The phonon properties depend on both the size effect (owing to the confinement effect of longitudinal optical phonons) and the surface state (owing to the formation of surface

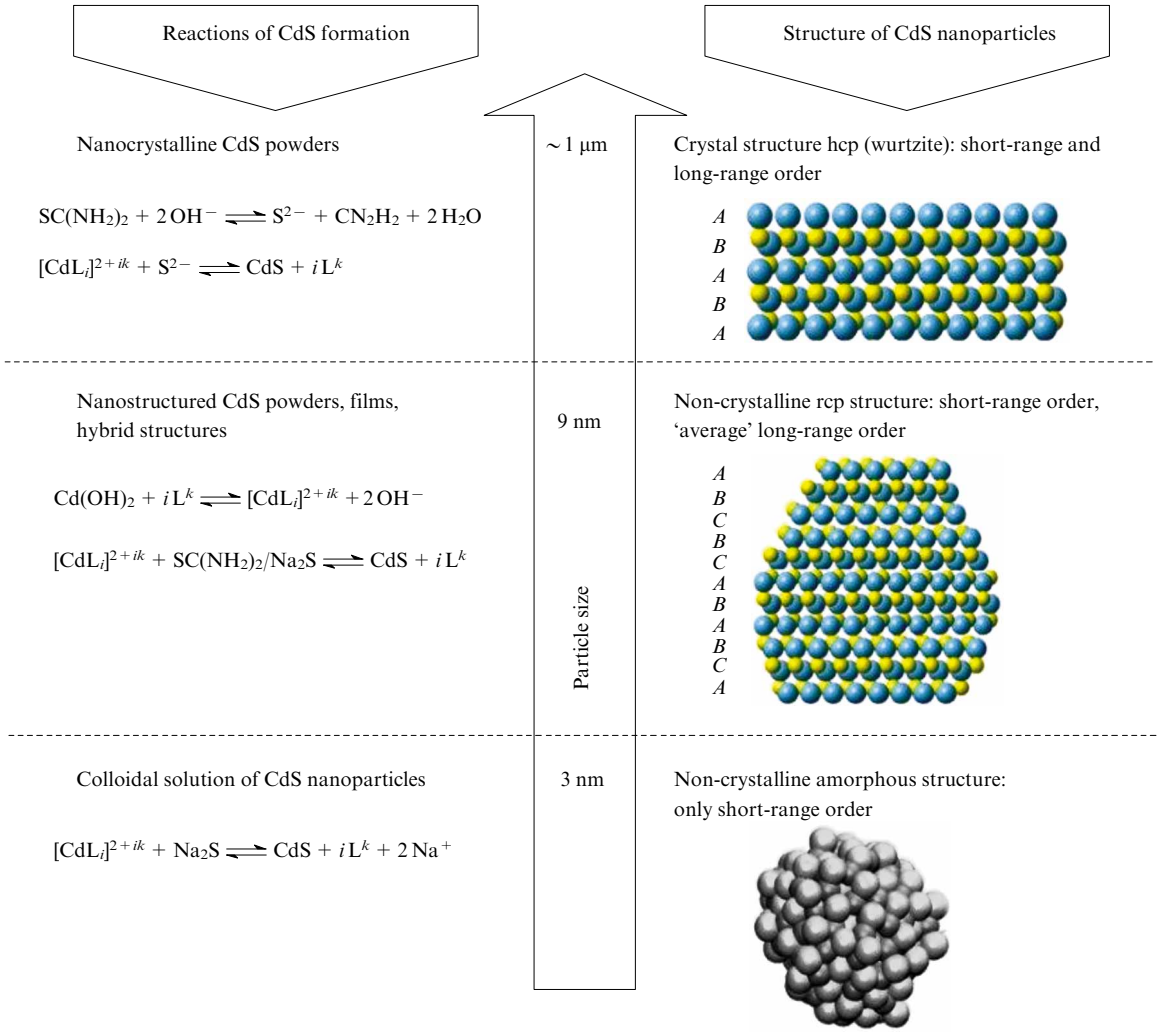


Figure 23. Formation conditions for different forms of CdS with different size of crystalline and non-crystalline nanoparticles taking into account the type of sulfidizer and the possibility of competing formation of $Cd(OH)_2$ (L is complex-forming agent).

modes). The magnetic susceptibility of CdS nanoparticles is determined by the dangling atom–atom bonds whose proportion depends on the atomic structure of the particle rather than the particle size. All these properties depend rather strongly on the particle size (diameter) or on the proportion of surface atoms in the particle. The internal structure of particles is also governed by the increased surface-to-volume ratio. In particular, disordering of packing layers in the rcp structure of small particles leads to a decrease in the proportion of surface bonds and thus provides an explanation for the appearance of random packing of layers in the nanostructured forms of CdS.

The luminescent properties of CdS nanoparticles depend on the size, structural and surface factors in the most complicated manner. Surface traps, electron–phonon coupling and nonradiative Auger processes lead to degradation of luminescence, blinking of luminescence and red shift of luminescence maxima. Suppression of nonradiative Auger processes and reduction of the effect of surface traps are possible for magic-size particles [107] characterized by noticeable blue shift and a rather high quantum yield.[112]

The first expectations of using CdS nanoparticles as quantum dots with a blue shift of luminescence and high quantum yield appeared to be overestimated. Long-term research was required to clarify the nature of processes accompanying luminescence. At present, one can state that the desired luminescent properties of CdS quantum dots can be achieved using ultrafine synthesis aimed at controlling the particle size and surface passivation. Luminescence in quantum dots is necessary for producing biolabels and colouring DNA molecules. When quantum dots are used in photocatalysis and for sensitization of solar cells, their luminescent properties are of no concern. Critical to these applications is the quantum yield of quantum dots which can be increased taking into account the influence of Auger processes and surface states. Among various methods for the synthesis of CdS particles for the aforesaid applications, CBD seems to be the best. As applied to the design of biomarkers, this method excludes the influence of harsh organic media on biological structures. Considering power engineering applications, the cost of the method and products of possible side reactions are of great importance. In this respect, CBD stands apart as cheap and safe method.

References

1. G A Kitaev, Doctoral Thesis in Chemical Sciences, Ural Polytechnic Institute, Sverdlovsk, 1971
2. S G Mokrushin, Yu D Tkachev *Kolloid. Zh.* **23** 438 (1961) [a]
3. G A Kitaev, A A Uritskarya, S G Morkrushin *Russ. J. Phys. Chem.* **39** 1101 (1965) [*Zh. Fiz. Khim.* **39** 2065 (1965)]
4. G A Kitaev, S G Mokrushin, A A Uritskaya *Kolloidn. Zh.* **27** 51 (1965) [a]
5. G A Kitaev, T P Bol'shchikova, G M Fofanov, L E Yatlova, N M Goryukhina, in *Kinetika i Mekhanizm Obrazovaniya Tverdoi Fazy* (Kinetics and Methanism of Solid Phase Formation) No. 170 (Sverdlovsk: Ural Polytechnic Institute, 1968) p. 113
6. M Bär, L Weinhardt, C Heske, H-J Muffler, E Umbach, M C Lux-Steiner, T P Niesen, F Karg, C-H Fischer *Solar Energy Mater. Solar Cells* **90** 3151 (2006)
7. S A Gavrilov, A A Sherchenkov, A B Apal'kov, D A Kravchenko *Ros. Nanotekhnol.* **1** 228 (2006) [b]
8. M H Badawi, S Aboul-Enein, M Ghali, G Hassan *Renew. Energy* **14** 107 (1998)
9. G Sasikala, P Thilakan, C Subramanian *Solar Energy Mater. Solar Cells* **62** 275 (2000)
10. I Repins, M A Contreras, B Egaas, C DeHart, J Scharf, C L Perkins, B To, R Noufi *Prog. Photovolt: Res. Appl.* **16** 235 (2008)
11. H Gleiter *Acta Mater.* **48** 1 (2000)
12. V A Oleinikov, A V Sukhanova, I R Nabiev *Ros. Nanotekhnol.* **2** 160 (2007) [b]
13. A I Khrebtov, V G Talalaev, P Werner, V V Danilov, M V Artemyev, B V Novikov, I V Shtrom, A S Panfutova, G E Cirlin *Semiconductors* **47** 1346 (2013) [*Fiz. Tekhn. Poluprovod.* **47** 1356 (2013)]
14. C B Murray, C R Kagan *Annu. Rev. Mater. Sci.* **30** 545 (2000)
15. D Valerini, A Creti, M Lomascolo, L Manna, R Cingolani, M Anni *Phys. Rev. B* **71** 235409 (2005)
16. A O Orlova, Y A Gromova, A V Savelyeva, V G Maslov, M V Artemyev, A Prudnikau, A V Fedorov, A V Baranov *Nanotechnology* **22** 455201(2011)
17. G I Tselikov, V Yu Timoshenko, J Plenge, E Rühl, A M Shatalova, G A Shandryuk, A S Merkalov, R V Tal'roze *Semiconductors* **47** 647 (2013)] *Fiz. Tekhn. Poluprovod.* **47** 633 (2013)
18. M Bruchez Jr, M Moronne, P Gin, S Weiss, A P Alivisatos *Science* **281** 2013 (1998)
19. C W Warren, C Nie, S Nie *Science* **281** 2016 (1998)
20. B Dubertret, P Skourides, D J Norris, V Noireaux, A H Brivanlou, A Libchaber *Science* **298** 1759 (2002)
21. A Sukhanova, L Venteo, J Devy, M Artemyev, V Oleinikov, M Pluot, I Nabiev *Lab. Invest.* **82** 1259 (2002)
22. V A Oleinikov *Priroda* (3) 22 (2010)
23. H S Mansur, A A P Mansur *J. Mater. Chem.* **22** 9006 (2012)
24. P Sharma, S Brown, G Walter, S Santra, B Moudgil *Adv. Colloid. Interface Sci.* **123–126** 471 (2006)
25. C Frigerio, D S M Ribeiro, S S M Rodrigues, V L R G Abreu, J A C Barbosa, J A V Prior, K L Marques, J L M Santos *Anal. Chim. Acta* **735** 9 (2012)
26. I Nabiev, S Mitchell, A Davies, Y Williams, D Kelleher, R Moore, Y K Gun'ko, S Byrne, Y P Rakovich, J F Donegan, A Sukhanova, J Conroy, D Cottell, N Gaponik, A Rogach, Y Volkov *Nano Lett.* **7** 3452 (2007)
27. Y Williams, A Sukhanova, M Nowostawska, A M Davies, S Mitchell, V Oleinikov, Y Gun'ko, I Nabiev, D Kelleher, Y Volkov *Small* **5** 2581 (2009)
28. F M Winnik, D Maysinger *Acc. Chem. Res.* **43** 672 (2013)
29. J-M Moulis, F Thevenod *Biometals* **23** 763 (2010)
30. G Schoeters, E den Hond, M Zuurbier, R Naginiene, P van den Hazel, N Stilianakis, R Ronchetti, J G Koppe *Acta Pediat.* **95** Suppl. 453 50 (2006)
31. C Kirchner, T Liedl, S Kudera, T Pellegrino, A M Javier, H E Gaub, S Stolzle, N Fertig, W J Parak *Nano Lett.* **5** 331 (2005)
32. Q Wang, P Liu, X Zhou, X Zhang, T Fang, P Liu, X Min, X Li *J. Photochem. Photobiol. A* **230** 23 (2012)
33. L Ye, K-T Yong, L Liu, I Roy, R Hu, J Zhu, H Cai, W-C Law, J Liu, K Wang, J Liu, Y Liu, Y Hu, X Zhang, M T Swihart, P N Prasad *Nat. Nanotechnol.* **7** 453 (2012)
34. G-S Li, D-Q Zhang, J C Yu *Environ. Sci. Technol.* **43** 7079 (2009)
35. L M Nikolenko, V F Razumov *Russ. Chem. Rev.* **82** 429 (2013)
36. C-Y Chen, M Wang, J-Y Li, N Pootrakulchote, L Alibabaei, C Ngoc-le, J D Decoppet, J-H Tsai, C Grätzel, C-G Wu, S M Zakeeruddin, M Grätzel *ACS Nano* **3** 3103 (2009)
37. H K Jun, M A Careem, A K Arof *Renew. Sustain. Energy Rev.* **22** 148 (2013)
38. H J Lee, P Chen, S-J Moon, F Sauvage, K Sivula, T Bessho, D R Gamelin, P Comte, S M Zakeeruddin, S I Seok, M Grdtzel, M K Nazeeruddin *Langmuir* **25** 7602 (2009)
39. S Emin, S P Singh, L Han, N Satoh, A Islam *Solar Energy* **85** 1264 (2011)
40. A G Kontos, V Likodimos, E Vassalou, I Kapogianni, Y S Raptis, C Raptis, P Falaras *Nanoscale Res. Lett.* **6** 266 (2011)
41. B D Hall, D Zanchet, D Ugarte *J. Appl. Cryst.* **33** 1335 (2000)
42. N V Klobukow *Z. Prakt. Chem.* **39** 413 (1889)
43. F Ulrich, W Zachariasen *Z. Kristallogr.* **62** 270 (1925)
44. H Metin, R Esen *J. Cryst. Growth* **258** 141 (2003)
45. M Rusu, A Rumberg, S Schuler, S Nishiwaki, R Wurz, S M Babu, M Dziedzina, C Kelch, S Siebentritt, R Klenk, T Schedel-Niedrig, M C Lux-Steiner *J. Phys. Chem. Sol.* **64** 1849 (2003)
46. O Conde, A G Rolo, M J M Gomes, C Riccoleau, D J Barber *J. Cryst. Growth* **247** 371 (2003)
47. B Su, M Wei, K L Choy *Mater. Lett.* **47** 83 (2001)
48. K Senthil, D Mangalaraj, S K Narayandass, R Kesavamoorthy, G L N Reddy, B Sundaravel *Physica B* **304** 175 (2001)
49. H El Maliki, J C Berne'de, S Marsillac, J Pinel, X Castel, J Pouzet *Appl. Surf. Sci.* **205** 65 (2003)
50. P N Gibson, M E Oezsan, D Lincot, P Cowache, D Summa *Thin Solid Films* **361** 34 (2000)
51. A I Oliva, R Castro-Rodríguez, O Ceh, P Bartolo-Perez, F Caballero-Briones, V Sosa *Appl. Surf. Sci.* **148** 42 (1999)
52. J Zhang, L Sun, S Liao, C Yan *Solid State Commun.* **124** 45 (2002)
53. A A Rempel, N S Kozhevnikova, S Van den Berge, W Van Renterghem, A J G Leenaers *Phys. Status Solidi, B* **242** R61 (2005)
54. W Wang, Z Liu, C Zheng, C Xu, Y Liu, G Wang *Mater. Lett.* **57** 2755 (2003)
55. D Pan, S Jiang, L An, B Jiang *Adv. Mater.* **16** 982 (2004)
56. G S Wu, X Y Yuan, T Xie, G C Xu, L D Zhang, Y L Zhuang *Mater. Lett.* **58** 794 (2004)
57. C Li, X Yang, B Yang, Y Yan, Y Qian *J. Cryst. Growth* **291** 45 (2006)
58. C Chen, C Zhu, L Hao, Y Hu, Z Chen *Inorg. Chem. Commun.* **7** 322 (2004)
59. A S Vorokh, A A Rempel *Phys. Solid State* **49** 148 (2007) [*Fiz. Tv. Tela* **49** 143 (2007)]
60. A S Vorokh, A A Rempel *Dokl. Phys.* **52** 200 (2007) [*Dokl. Akad. Nauk, Ser. Fiz.* **413** 743 (2007)]
61. A S Vorokh, A A Rempel *J. Exp. Theor. Phys. Lett.* **91** 100 (2010) [*Pis'ma Zh. Eksp. Teor. Fiz.* **91** 102 (2010)]
62. C E Junkermeier, J P Lewis, G W Bryant *Phys. Rev. B* **79** 125323 (2009)
63. A F Andrushko *Fiz. Tv. Tela* **4** 582 (1962) [c]

64. R Xu, Y Wang, G Jia, W Xu, S Liang, D Yin *J.Cryst. Growth* **299** 28 (2007)
65. G Z Wang, Y W Wang, W Chen, C H Liang, G H Li, L D Zhang *Mater. Lett.* **48** 269 (2001)
66. Y C Zhang, G Y Wang, X Y Hu *J. Alloys Compd.* **437** 47 (2007)
67. X C Wu, Y R Tao *J. Cryst. Growth* **242** 309 (2002)
68. Z Li, Y Du, Z Zhang, D Pang *React. Funct. Polym.* **55** 35 (2003)
69. K S Ramaiah, R D Pilkington, A E Hill, R D Tomlinson, A K Bhatnagar *Mater. Chem. Phys.* **68** 22 (2001)
70. T Yoshida, K Yamaguchi, T Kazitani, T Sugiura, H Minoura *J. Electroanal. Chem.* **473** 209 (1999)
71. N I Fainer, Yu M Rumyantsev, M L Kosinova, S M Zemskova, E A Maximovskiy, G S Yurjev, G F Sivykh *Nucl. Instr. Methods Phys. Res., Sect. A* **448** 290 (2000)
72. P Christian, P O Brien *Chem. Commun.* 2817 (2005)
73. M Rami, E Benamar, M Fahoume, F Chraibi, A Ennaoui *Solid State Sci.* **1** 179 (1999)
74. J N Ximello-Quiebras, G Contreras-Puente, J Aguilar-Hernandez, G Santana-Rodriguez, A A C Readigos *Solar Energy Mater. Solar Cells* **82** 263 (2004)
75. C Ricolleau, L Audinet, M Gandais, T Gacoin, J P J Boilot *J. Cryst. Growth* **203** 486 (1999)
76. O V Kovalev *Neprivodimye i Indutsirovannye Predstavleniya i Kopredstavleniya Fedorovskikh Grupp* (Irreducible and Induced Representations and Corepresentations of Fedorov Groups) (Moscow: Nauka, 1986)
77. A P Alivisatos *Science* **271** 933 (1996)
78. A I Ekimov, A A Onushchenko *Pis'ma Zh. Eksp. Teor. Fiz.* **40** 337 (1984) [d]
79. Al L Efros, A L Efros *Fiz. Tekhn. Poluprov.* **16** 1209 (1982) [e]
80. L E Brus *J. Chem. Phys.* **80** 4403 (1984)
81. S Sapra, D D Sarma *Phys. Rev. B* **69** 125304 (2004)
82. A Nazzal, H Fu *J. Comp. Theor. Nanosci.* **6** 1277 (2009)
83. J Luning, J Rockenberger, S Eisebitt, J-E Rubenssona, A Karl, A Kornowski, H Weller, W Eberhardt *Solid State Commun.* **112** 5 (1999)
84. D Schoob, A Mews, A Eychmuller, H Weller *Phys. Rev. B* **49** 17072 (1994)
85. P E Lippens, M Lannoo *Phys. Rev. B* **39** 10935 (1989)
86. A G Milekhin, L L Sveshnikova, S M Repinskii, A K Gutakovskii, M Fridrikh, D R T Zahn *Phys. Solid State* **44** 1976 (2002) [*Fiz. Tv. Tela* **44** 1884 (2002)]
87. S Biswas, M Dutta, P Snee, M A Stroscio *Chin. J. Phys.* **49** 92 (2011)
88. P Kumar, N Saxena, F Singh, A Agarwal *Physica B* **407** 3347 (2012)
89. A Singha, B Satpati, P V Satyam, A Roy *J. Phys.: Condens. Matter* **17** 5697 (2005)
90. V Dzhagan, M Valakh, N Melnik, O Rayevska, I Lokteva, J Kolny-Olesiak, D R T Zahn *Int. J. Spectrosc.* 532385 (2012)
91. A Aresti, P Manca, A Spiga *J. Phys. C: Solid State Phys.* **12** 3795 (1979)
92. S V Vonsovskii *Magnetizm* (Magnetism) (Moscow: Nauka, 1971)
93. A S Vorokh, S Z Nazarova, N S Kozhevnikova *Phys. Solid State* **54** 1306 (2012) [*Fiz. Tv. Tela* **54** 1228 (2012)]
94. M F Kotkata, A E Masoud, M B Mohamed, E A Mahmoud *Physica E* **41** 1457 (2009)
95. E Buressi, M Celino *Solid State Sci.* **14**567 (2012)
96. N Pinna, K Weiss, J Urban, M P Pileni *Adv. Mater.* **13** 261 (2001)
97. A A Klochikhin, S A Permogorov, A N Reznitskii *Fiz. Tv. Tela* **39** 1170 (1997) [c]
98. C Barglik-Chory, D Buchold, M Schmitt, W Kiefer, C Heske, C Kumpf, O Fuchs, L Weinhardt, A Stahl, E Umbach, M Lentze, J Geurts, G Mueller *Chem. Phys. Lett.* **379** 443 (2003)
99. M Majumder, A K Chakraborty, B Mallik *J. Luminesc.* **130** 1497 (2010)
100. Y R Wang, C B Duke *Phys. Rev. B* **37** 6417 (1988)
101. S Gorer, J A Ganske, J C Hemminger, R M Penner *J. Am. Chem. Soc.* **120** 9584 (1998)
102. A V Katsaba, S A Ambrozevich, A G Vitukhnovsky, V V Fedyanin, A N Lobanov, V S Krivobok, R B Vasiliev, I G Samatov *J. Appl. Phys.* **113** 184306 (2013)
103. K Sato, S Kojima, S Hattori, T Chiba, K Ueda-Sarson, T Torimoto, Y Tachibana, S Kuwabata *Nanotechnology* **18** 465702 (2007)
104. M Marandi, N Taghavinia, A Iraji zad, S M Mahdavi *Nanotechnology* **17** 1230 (2006)
105. E A Bagaev, K S Zhuravlev, L L Sveshnikova, I A Badmaeva, S M Repinskii, M Voelskow *Semiconductors* **37** 1321 (2003) [*Fiz. Tekhn. Poluprovod.* **37** 1358 (2003)]
106. M V Artemyev, V Sperling, U Woggon *J. Appl. Phys.* **81** 6975 (1997)
107. G E Cragg, Al L Efros *Nano Lett.* **10** 313 (2010)
108. A W Cohn, A M Schimpf, C E Gunthardt, D R Gamelin *Nano Lett.* **13** 1810 (2013)
109. C Javaux, B Mahler, B Dubertret, A Shabaev, A V Rodina, Al L Efros, D R Yakovlev, F Liu, M Bayer, G Camps, L Biadala, S Buil, X Quelin, J-P Hermier *Nat. Nanotechnol.* **8** 206 (2013)
110. A Saha, K V Chellappan, K S Narayan, J Ghatak, R Datta, R Viswanatha *J. Phys. Chem. Lett.* **4** 3544 (2013)
111. A W Cohn, J D Rinehart, A M Schimpf, A L Weaver, D R Gamelin *Nano Lett.* **14** 353 (2014)
112. M Li, J Ouyang, C I Ratcliffe, L Pietri, X Wu, D M Leek, I Moudrakovski, Q Lin, B Yang, K Yu *ACS Nano* **3** 3832 (2009)
113. J Liebig *Ann. Pharm.* **14** 134 (1835)
114. C Puscher *Dingl. J.* **190** 421 (1869)
115. K L Chopra, S R Das *Thin Film Solar Cells* (New York: Plenum Press, 1983)
116. C D Lokhande *Mater. Chem. Phys.* **27** 1 (1991)
117. D Lincot, M Froment, H Cachet, in *Advances in Electrochemical Sciences and Engineering* Vol. 6 (Eds R C Alkire, D M Kolb) (New York; Wiley-VCH, 1999) p. 165
118. P O'Brien, J McAleese *J. Mater. Chem.* **8** 2309 (1998)
119. P K Nair, M T S Nair, V M Garcia, O L Arenas, Y Pena, A Castillo, I T Ayala, O Gomezdaza, A Sanchez, J Campos, H Hu, R Suarez, M E Rincon *Solar Energy Mater. Solar Cells* **52** 313 (1998)
120. O Savadogo *Solar Energy Mater. Solar Cells* **52** 361 (1998)
121. R S Mane, C D Lokhande *Mater. Chem. Phys.* **65** 1 (2000)
122. C D Lokhande, P M Gondkar, R S Mane, V R Shinde, S-H Han *J. Alloys Compd.* **475** 304 (2009)
123. H Parikh, M R De Guire *J. Ceram. Soc. Jpn.* **117** 228 (2009)
124. T Kawano, N Imai *J. Ceram. Soc. Jpn.* **118** 969 (2010)
125. S M Pawar, B S Pawar, J H Kim, O-S Joo, C D Lokhande *Curr. Appl. Phys.* **11** 117 (2011)
126. T P Niesen, M R De Guire *J. Electroceram.* **6** 169 (2001)
127. G Hodes *Phys. Chem. Chem. Phys.* **9** 2181 (2007)
128. I Prigogine, R Defay *Chemical Thermodynamics* (Upper Saddle River, NJ.: Prentice Hall Press, 1954)
129. T De Donder, P Van Rysselberghe *Thermodynamic Theory of Affinity (A Book of Principles)* (Menlo Park, CA: Stanford University Press, 1936)
130. V F Markov, L N Maskaeva, P N Ivanov *Gidrokhimicheskoe Osazhdenie Plenok Sul'fidov Metallov: Modelirovanie i Eksperiment* (Hydrochemical Deposition of Metal Sulfide Films: Modelling and Experiment) (Ekaterinburg: Ural Branch, Russian Academy of Science, 2006)
131. B Mertschenk, F Beck, W Bauer, in *Ullmann's Encyclopedia of Industrial Chemistry* (Weinheim: Wiley-VCH, 2005) p. 1
132. D Hariskosa, M Powalla, N Chevaldonnet, D Lincot, A Schindler, B Dimmler *Thin Solid Films* **387** 179 (2001)
133. W H R Shaw, D G Walker *J. Am. Chem. Soc.* **78** 5769 (1956)

134. G A Kitaev, A A Uritskaya, L E Yatlova, V R Mirolyubov *Zh. Prikl. Khim.* **67** 1612 (1994) [f]
135. N P Volynskii *Tiosernaya Kislota. Politionaty: Reaktsiya Vakenrodera* (Thiosulfuric Acid. Polythionates: Wackenroder's Reaction) (Moscow: Nauka, 1971)
136. G A Kitaev, A A Uritskaya *Zh. Prikl. Khim.* **72** 569 (1999) [f]
137. G A Kitaev, A A Uritskaya, N S Belova *Zh. Prikl. Khim.* **73** 1433 (2000) [f]
138. P U Bhaskar, G S Babu, Y B K Kumar, Y Jayasree, V S Raja *Mater. Chem. Phys.* **134** 1106 (2012)
139. E H Swift, E A Butler *Anal. Chem.* **28** 146 (1956)
140. E A Butler, D G Peters, E H Swift *Anal. Chem.* **30** 1379 (1958)
141. T Sugimoto, G E Dirige, A Muramatsu *J. Colloid Interface Sci.* **176** 442 (1995)
142. G Hodes *Chemical Solution Deposition of Semiconductor Films* (New York: Marcel Dekker, 2002)
143. M Froment, D Lincot *Electrochim. Acta* **40** 1293 (1995)
144. J M Dona, J Herrero *J. Electrochem. Soc.* **144** 4081 (1997)
145. A S Katysheva, V F Markov, L N Maskaeva *Russ. J. Inorg. Chem.* **58** 833 (2013) [*Zh. Neorg. Khim.* **58** 940 (2013)]
146. N S Kozhevnikova, A A Uritskaya, A S Vorokh, A A Rempel *Russ. J. Gen. Chem.* **78** 551 (2008) [*Zh. Obshch. Khim.* **78** 568 (2008)]
147. A A Uritskaya, G A Kitaev, N S Belova *Zh. Prikl. Khim.* **75** 864 (2002) [f]
148. N S Belova, A A Uritskaya, G A Kitaev *Zh. Prikl. Khim.* **75** 1598 (2002) [f]
149. A A Uritskaya, T P Bol'shchikova, N S Kozhevnikova *Russ. J. Gen. Chem.* **77** 818 (2007) [*Zh. Obshch. Khim.* **77** 717 (2007)]
150. R Ortega-Borges, D Lincot *J. Electrochem. Soc.* **140** 3464 (1993)
151. A S Vorokh, N S Kozhevnikova, A A Rempel, A Magerl *J. Struct. Chem.* **51** 1170 (2010) [*Zh. Strukt. Khim.* **51** 1206 (2010)]
152. A T Nabiev, R D Asadullina, S V Pestrikov, A A Gashnikova, K R Khamat'yarova *Bashk. Khim. Zh.* **16** 145 (2009)
153. N S Kozhevnikova, A A Rempel, F Hergert, A Magerl *Thin Solid Films* **517** 2586 (2009)
154. C A Barboza, J M Henriques, E L Albuquerque, V N Freire, J A P da Costa, E W S Caetano *J. Phys. D: Appl. Phys.* **42** 155406 (2009)
155. D Vollath *Nanomaterials: an Introduction to Synthesis, Properties and Applications* (Weinheim: Wiley-VCH, 2008)
156. N S Kozhevnikova, A A Uritskaya, A A Rempel *Dokl. Phys. Chem.* **453** 270 (2013) [*Dokl. Akad. Nauk, Ser. Fiz. Khim.* **453** 167 (2013)]
157. V S Shinde, T P Gujar, T Noda, D Fujita, C D Lokhande, O-S Joo *J. Phys. Chem. C* **113** 14179 (2009)
158. H Zeng, P M Rice, S X Wang, S Sun *J. Am. Chem. Soc.* **126** 11458 (2004)
159. A S Vorokh, N S Kozhevnikova, A A Uritskaya, A Magerl *Russ. J. Phys. Chem.* **82** 1132 (2008) [*Zh. Fiz. Khim.* **82** 1282 (2008)]
160. A S Vorokh, S Z Nazarova, N S Kozhevnikova *Mendeleev Commun.* **24** 55 (2014)
161. A S Vorokh, S Z Nazarova, N S Kozhevnikova *Dokl. Phys. Chem.* **454** 21 (2014) [*Dokl. Akad. Nauk, Ser. Fiz. Khim.* **454** 300 (2014)]
162. T Sugimoto, G E Dirige, A Muramatsu *J. Colloid Interface Sci.* **173** 257 (1995)
163. T Sugimoto, G E Dirige, A Muramatsu *J. Colloid Interface Sci.* **182** 444 (1996)
164. A S Vorokh, N S Kozhevnikova *Dokl. Phys. Chem.* **419** 41 (2008) [*Dokl. Akad. Nauk, Ser. Fiz. Khim.* **419** 58 (2008)]
165. C B Murray, D J Norris, M G Bawendi *J. Am. Chem. Soc.* **115** 8706 (1993)
166. S Kim, M G Bawendi *J. Am. Chem. Soc.* **125** 14652 (2003)
167. D Gerion, F Pinaud, S C Willimas, W J Parak, D Zanchet, S Weiss, A P Alivisatos *J. Phys. Chem. B* **105** 8861 (2001)
168. L Ma, S-M Wu, J Huang, Y Ding, D-W Pang, L Li *Chromosoma* **117** 181 (2008)
169. X Gao, Y Cui, R M Levenson, L W K Chung, S Nie *Nat. Biotechnol.* **22** 969 (2004)
170. Y-C Chu, C-C Wang, C-Y Chen *Nanotechnology* **16** 58 (2005)
171. S H Liu, X F Qian, J Yin, X D Ma, J Y Yuan, Z K Zhu *J. Phys. Chem. Solids* **64** 455 (2002)
172. K Sooklal, L H Hanus, H J Ploehn, C J Murphy *Adv. Mater.* **10** 1083 (1998)
173. E D Spoerke, J A Voigt *Adv. Funct. Mater.* **17** 2031 (2007)
174. L Zou, Z Fang, Z Gu, X Zhong *J. Luminecs.* **129** 536 (2009)
175. Z Zhuang, X Lu, Q Peng, Y Li *J. Am. Chem. Soc.* **132** 1891 (2010)
176. E Gabellieri, P Cioni, E Balestreri, E Morelli *Eur. Biophys. J.* **40** 1237 (2011)
177. S M M Nelwamondo, M J Moloto, R W Krause, N Moloto *Mater. Res. Bull.* **47** 4392 (2012)
178. P Huang, Q Jiang, P Yu, L Yang, L Mao *ACS Appl. Mater. Interfaces* **5** 5239 (2013)
179. N S Kozhevnikova, A S Vorokh, A A Rempel *Russ. J. Gen. Chem.* **80** 391 (2010) [*Zh. Obshch. Khim.* **80** 365 (2010)]
180. A A Rempel, N S Kozhevnikova, S V Rempel *Russ. Chem. Bull., Int.Ed.* **62** 398 (2013) [*Izv. Akad. Nauk, Ser. Khim.* **62** 400 (2013)]

[a] — *Colloid J. (Engl. Transl.)*
[b] — *Nanotechn. Russ. (Engl. Transl.)*
[c] — *Phys. Solid State (Engl. Transl.)*
[d] — *J. Exp. Theor. Phys. Lett. (Engl. Transl.)*
[e] — *Semiconductors (Engl. Transl.)*
[f] — *Russ. J. Appl. Chem. (Engl. Transl.)*